Determination of Thallium and Indium with an Electrochemically-reduced Graphene Oxide-Carbon Paste Electrode by Anodic Stripping Voltammetry

A thesis submitted in fulfilment of the requirements for the degree of

Magister Scientiae in Nanoscience (Chemistry)

Department of Chemistry: Sensor Lab

University of Western Cape

Supervisor: Prof N. Jahed

Co-supervisor: Prof E.I. Iwuoha

by

Tayla Martin

Keywords

Trace Metal Analysis

Heavy Metal Detection

Mercury film

Carbon Paste Electrode

Square Wave Anodic Stripping Voltammetry

Electrochemical Reduction

Chemical Sensor

Abstract

In this study, graphene oxide was synthesized by oxidizing graphite using the modified Hummer's method. The graphene oxide was characterized by Raman Spectroscopy, Fourier Transform Infrared Spectroscopy, High Resolution Transmission Electron Microscopy, Scanning Electron Microscopy and X-Ray Diffraction for structural and morphological properties.

The graphene oxide was electrochemically reduced on a carbon paste electrode followed by the *in situ* deposition of mercury thin films to achieve electrochemically reduced graphene oxide modified carbon paste metal film electrodes (ERGO-CP-MEs).

The experimental parameters (amplitude, deposition time, deposition potential, frequency and rotation speed) were optimized, and the applicability of the modified electrode was investigated towards the simultaneous and individual determination of TI^{1+} and In^{3+} at the low concentration levels ($\mu g\ L^{-1}$) in 0.1 M acetate buffer (pH 4.6) using square wave anodic stripping voltammetry (SWASV). The detection limit values for individual analysis at electrochemically reduced graphene oxide modified carbon paste mercury film electrode (ERGO-CP-HgE) was 2.4 and 1.1 $\mu g\ L^{-1}$ for TI^{1+} and In^{3+}, respectively. The detection limit values for simultaneous analysis at ERGO-CPE was 1.32 and 1.33 $\mu g\ L^{-1}$ and individual analysis was 0.975 and 1.04 $\mu g\ L^{-1}$ for TI^{1+} and In^{3+}, respectively.

Real sample analysis was done with laboratory tap water using the voltammetric sensor proved to be suitable for the detection of heavy metals below the United States Environmental Protection Agency (US EPA) prescribed water standards of 2 and 0.07 mg mL^{-1} for TI^{1+} and In^{3+}, respectively.

Declaration

I declare that the study "**Determination of Thallium and Indium with an Electrochemically-Reduced Graphene Oxide modified Carbon Paste Electrode by Anodic Stripping Voltammetry**" is my own work. It has not been submitted for any degree or examination in any university, and all the resources I have used or quoted have been indicated and acknowledged by complete references.

Tayla Martin March 2018

Acknowledgements

To my supervisor, Dr. Nazeem Jahed, thank you for your guidance, endless insight, encouragement and support.

I would like to thank Dr K. Pokpas for your diligence, endless discussions, laughs and continuous support.

I would like to extend my gratitude to Prof.E. Iwuoha, Prof. P. Baker, the co-chairs of SensorLab and to all the Sensor Lab members and staff, as well as UWC chemistry department staff. Thank you for the opportunity and trust placed in me.

Lastly, to my friends and family for the unwavering support, laughs and cries. Thank you for all the encouragement. Without you this would not be possible.

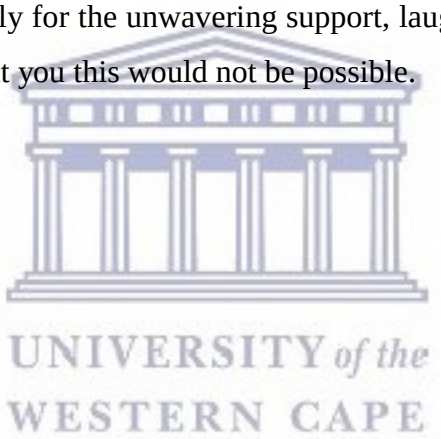

List of Abbreviations

AdSV	Adsorptive stripping voltammetry
ASV	Anodic stripping voltammetry
AAS	Atomic absorption spectroscopy
BiFE	Bismuth film electrode
CPE	Carbon paste electrode
CSV	Cathodic stripping voltammetry
CV	Cyclic voltammetry
DPV	Differential pulse voltammetry
EDS	Electronic data system
EDTA	Ethylenediaminetetraacetic acid
ERGO	Electrochemically reduced graphene oxide
ERGO-CP-MEs	Electrochemically reduced graphene oxide modified carbon paste metal electrodes
ERGO-CP-HgEs	Electrochemically reduced graphene oxide modified carbon paste mercury film electrodes
FAAS	Flame atomic absorption spectroscopy
FTIR	Fourier transform infrared spectroscopy
GCE	Glassy carbon electrode
GO	Graphene oxide
HMDE	Hanging mercury drop electrode
ICP-AES	Inductively coupled plasma atomic emission spectroscopy
ICP-OES	Inductively coupled plasma optical emission spectroscopy
ICP-MS	Inductively coupled plasma mass spectroscopy
MTFE	Mercury thin film electrode

N.D	Not determined
NPV	Normal pulse voltammetry
RSD	Relative standard deviation
SEM	Scanning electrode microscope
SV	Stripping voltammetry
SWASV	Square wave anodic stripping voltammetry
TEM	Transmission electrode microscope
US EPA	United States Environmental Protection Agency
XRD	X-ray diffraction

List of Figures

List of Tables

Table of Contents

Chapter One:

Introduction to the study

1.1 Problem Statement

The technological advances in the semiconductor industry have resulted in advance in touchscreen, computer chips, fibre optics devices [1] . However, the heavy metals found in these electronic devices are finding their way into the environment owing to incorrect disposal procedures. Analytical chemists are now faced with the task of conducting research into developing chemical analysis procedures for trace heavy metals.

Heavy metals are metallic elements which have an atomic weight greater than 40.04 atomic mass units and, enter the environment either by anthropogenic (soil erosion, mining, industrial discharge, pesticides applied to plants, etc.) or natural means [2].

Thallium and Indium is used in many applications in the environmental, electronic, clinical and industrial fields [3]. In the United States, Thallium is mainly used in the electronic industry [4] for the production of special glass whereas, Indium is used for the production of photovoltaics and liquid crystal displays [1]. Owing to the popularity of electronic devices in Taiwan and Japan, the Japan Society for Occupational Health has set limits in the drinking water for Indium at 70 and at 3μg/L in serum [1].

According to United States Environmental Protection Agency (US-EPA), the maximum contaminant level for Thallium in drinking water is 2 ppm. The standard for World Health Organization for Thallium has not been reported. Exposure to Thallium toxicity originates from anthropogenic sources which run off into reservoirs.

Stripping voltammetry such as Anodic, Cathodic and Adsorptive voltammetric stripping are used to detect exceedingly low concentrations.

Stripping voltammetry at the hanging mercury drop electrode (HMDE) is capable of determining TI(I) in the 0.5 to 100 ppb range [5, 6] while the mercury film electrode in the 0.01-10 ppb range.

Mercury, antimony and bismuth films were previously prepared in-situ on glassy carbon electrodes and used to determine TI by anodic stripping voltammetry [6–8]. Metal film electrodes were also successfully used with chelating agents for example, EDTA to mask any Thallium interfering metals present in solution [9, 10]

Indium has been determined by hanging mercury drop electrode (HMDE) [9], bismuth film electrodes (BiFE) [10] and glassy carbon electrodes (GCE) [11]. However, the use of mercury has been reported due to its toxicity and alternative electrodes have been investigated such as glassy carbon electrode, carbon paste electrodes and screen-printed electrodes. Research on Thallium and Indium with carbon paste electrodes have not fully been investigated. However, it has been commonly used for organic, biological and other heavy metals.

1.2 Motivation to the study

Anodic stripping voltammetry is a powerful, analytical technique used for the determination of trace heavy metals in water such as Pb, Cu, Zn, Mn and Cd [12, 13]. The advantages of this technique includes high reproducibility, high sensitivity and low detection limits. The success of a stripping technique depends on the choice of working electrode [6].

Features, such as sensitivity and good reproducibility are ideal for electrode selection. Traditionally, hanging mercury electrodes and glassy carbon electrodes have been used for this reason. However, these electrodes are expensive. Carbon paste electrodes [4], screen printed electrodes and pencil electrodes [13] exhibit high sensitivity, environmentally friendly, cheap and easy to fabricate.

Carbon paste electrodes (CPE) was used as an alternative electrode to HMDE and GCE. These carbon paste electrodes were made from graphite powder and mineral oil as a binder. The contents were placed in different plastic containers. The advantage of this electrode was that it could be re-used as much as possible and its contents recycled. Heavy metals and organic species was successfully detected by using CPE. However, to improve the sensitivity, CPE was modified by adding graphene [14], graphene oxide [15], carbon black, montmorillonite clay [16, 17] gold nanoparticles [18] or heavy metals [19].

Thallium and Indium are commonly used in technological advances such as semi-conductors, fibre optics and touch screen devices [1]. Due to unsuitable waste removal techniques, these heavy metals are found in drinking water. Earlier analytical techniques such as inductively-coupled plasma-optical emission spectroscopy (ICP-OES), atomic absorption spectroscopy (AAS) and flame absorption spectroscopy (FAAS) have been used for trace analysis, however these techniques are quite costly and requires trained professionals.

Detection of these metals require techniques that can detect trace amounts in real samples such as stripping voltammetry. Research on anodic stripping was used extensively on detection of Indium and Thallium [6,7, 10, 20–23].

Thallium and Indium was detected by an Antimony film Carbon Paste Electrode with obtained detection limits of 1,4 and 2,4 μg L^{-1}, respectively [21]. According to our knowledge, research on carbon paste electrodes modified with graphene oxide for the determination of Thallium and Indium has not been investigated.

Hence in this work, Thallium and indium will be investigated by a carbon paste electrode modified with graphene oxide which will be electrochemically-reduced on the surface of the electrode. The effect of a mercury film *in situ* on thallium and indium was also investigated.

1.3 Objectives were to

- investigate and understand the Square-wave Voltammetry technique.
- prepare unmodified carbon paste electrodes and explore its response towards indium and thallium, individually and simultaneously.
- synthesize Graphene oxide by the modified Hummer's method.
- characterize graphene oxide by Raman spectroscopy, X-ray diffraction (XRD), high resolution transmission electron microscopy (HR-TEM), scanning electron microscopy (SEM) and Fourier Transform Infrared Spectroscopy (FTIR).
- electrochemically reduce Graphene oxide via Cyclic Voltammetry and deposit onto the surface of the electrode
- detect thallium and indium by Electrochemically-reduced Graphene oxide modified carbon paste electrode (ERGO-CPE), individually and simultaneously.
- detect thallium and indium by Electrochemically-reduced Graphene oxide modified carbon paste electrode *in situ* on a mercury film (ERGO-CP-HgE), individually.
- study simultaneous detection of thallium and indium by ERGO-CP-HgE
- conduct recovery studies to confirm the accuracy of the analysis in test solutions and real sample analysis

1.4 Research Questions

- Would carbon paste electrodes be suitable in trace metal analysis?
- Would modifiers such as electrochemically-reduced graphene oxide enhance electrode sensitivity in analysis or determination of trace metal concentrations?
- Do graphene oxide modified electrodes offer comparable results to other graphene oxide electrodes in terms of detection limits and recoveries for real water samples?

1.5 Hypothesis

Is it possible to improve the sensitivity and detection limits of carbon paste electrodes to below the USEPA standards of Thallium at 2 mg L^{-1} and for Indium in drinking water at 0.07 mg L^{-1}, using graphene oxide modified electrode in square-wave anodic stripping voltammetry (SWASV).

1.6 Thesis Outline

1.6.1 Chapter One: Introduction to the study

Chapter one gives an introduction to the rationale, motivation of the study, objectives that need to be met, research questions and hypothesis.

1.6.2 Chapter Two: Literature review

Chapter two reviews previous research focussing on Stripping voltammetry and their different types, the different types of electrodes, common voltammetric techniques, graphene and nanoscience.

1.6.3 Chapter Three: Methodology

Chapter three outlines the equipment and procedure used in this work for graphene oxide synthesis. The electrode preparation was also included as well as the SWASV procedure.

1.6.4 Chapter Four: Morphological and Structural Characterization of Graphene oxide

Chapter four discusses the morphological and structural characterization of graphene oxide by microscopic and spectroscopic techniques.

1.6.5 Chapter Five: Electrochemically-reduced deposited graphene oxide carbon paste electrode (ERGO-CPE)

Chapter five reports results and discussion. ERGO-CPE are prepared by GO solutions. Instrumental parameters, calibration data, standard addition method in test solutions, real water samples were highlighted and interference studies. Detection limits, relative standard deviation (RSD) and recoveries (%) were reported.

1.6.6 Chapter Six: Electrochemically-reduced deposited graphene oxide carbon paste electrode *in situ* plated mercury film electrode (ERGO-CP-HgE)

Chapter six reports results and discussion similarly to ERGO-CP-HgE. This chapter includes influence of the mercury film on the trace metals. Instrumental parameters, calibration data, standard addition method in test solutions and real water samples were highlighted. Detection limits, relative standard deviation (RSD) and recoveries (%) were reported. Interference studies were also conducted

1.6.7 Chapter Seven: Conclusions and Future work

Chapter seven confirms the hypothesis in this research based on the results and discussion of the previous two chapters. Conclusions are discussed and future work is highlighted.

Chapter Two:

Literature review

2.1 Introduction

This chapter outlines the different electroanalytical techniques that is used for the detection of Thallium and Indium. It also focuses on the different electrodes that has been used previously in research. Nanoscience and Graphene is also highlighted in this chapter.

2.2 Stripping Voltammetry Techniques

Various techniques and methods such as atomic absorption spectrometry (AAS), flame atomic absorption spectrometry (FAAS), inductively coupled plasma mass spectrometry (ICP-MS), inductively coupled plasma atomic emission spectrometry (ICP-AES) and inductively coupled plasma optical emission spectrometry (ICP-OES) have been used for trace metal determination, however these techniques are expensive, time consuming and require trained personnel [24], [25].

Stripping Voltammetry is a highly sensitive and low cost analytical technique used to determine metal cations, organic and inorganic species in low concentrations at mg L^{-1}, μg L^{-1} and ng L^{-1} range [26, 27].

The pre-concentration or deposition step is vital in stripping voltammetry analysis. It involves deposition of the analyte atoms or molecules onto the electrode surface by applying a given potential (positive or negative). The potential applied depends on the analyte studied [13].

There are three types of stripping voltammetry techniques such as anodic stripping, cathodic stripping, adsorptive stripping voltammetry and potentiometric stripping voltammetry [27].

2.2.1 Anodic Stripping Voltammetry

Anodic stripping voltammetry (ASV) is an analytical technique used to detect metal cations [26, 27] in liquid media. Due to its high sensitivity, convenience and cost effectiveness it is possible to detect trace levels of metals in part-per million (ppm) and part-per-billion (ppb) range.

Various heavy metals can be determined by ASV such as antimony, arsenic, bismuth, cadmium, copper, gallium, germanium, manganese, indium, lead, mercury, silver, thallium, tin and zinc [10, 21, 25, 26, 28].

Anodic stripping voltammetry involves two steps, deposition and stripping step [30].

The deposition (pre-concentration) step involves applying a negative potential to the metals in solution onto the electrode surface in their metallic form. The aim of pre-concentration is to obtain lower limit of detection of the analyte [30].

$$M^{n+} + ne^- + Hg \rightarrow M(Hg)$$

The stripping step involves scanning the electrode linearly toward positive potentials to allow the metals to be stripped from the electrode surface and re-oxidized [28, 30].

$$M(Hg) \rightarrow M^{n+} + ne^- + Hg$$

During the deposition step, the working electrode behaves like a cathode and as an anode during the stripping step [30].

2.2.2 Cathodic Stripping Voltammetry

The procedure for cathodic stripping voltammetry (CSV) analysis is based on ASV principle, however the only difference is that the working electrode works like an anode in the deposition step and as a cathode in the stripping step. In comparison with ASV and Adsorptive stripping voltammetry (AdSV), CSV is rarely used for analysis [30].

Equation 2.1 $M \rightarrow M^{n+} + ne^-$ *(deposition step)(reduction step)*

$Mn^+ + A^{n-} \rightarrow MA$

Equation 2.2 $MA + ne^- \rightarrow M + A^{n-}$ *(stripping step)(oxidation step)*

Where;

M is metal

A is analyte

Organic compounds (nucleic acid bases) and inorganic anions (halides, selenide, sulfide, oxyanions), which form insoluble salts with mercury can be detected by CSV [30].

It has been used to determine heavy metals in sea water with complexing agents such as salicylaldoxime and 1-nitroso-2-napthol to enhance the detection limits of the analytes [30, 31].

2.2.3 Adsorptive Stripping Voltammetry

Adsorptive stripping voltammetry (AdSV) is similar to anodic and cathodic stripping methods. The primary difference is that the pre-concentration step of the analyte is obtained by adsorption on the electrode surface or by specific reactions at chemically modified electrodes rather than accumulation by electrolysis. Many organic and inorganic species have been determined at micromolar and nanomolar concentration levels using AdSV. Heavy metals such as aluminium, cadmium, chromium, cobalt, indium, iron, nickel and uranium can be detected by AdSV [9, 26, 32–35]. The adsorbed species is quantified by using a voltammetric technique such as DPV or SWV in either the negative or positive direction to give a peak-shaped voltammetric

response with amplitude proportional to concentration.

Complexing agents such as xylenol orange, morin, cupferron, catechol and pyrogallol red are commonly used in AdSV to enhance detection limits of heavy metals such as Indium, Gallium and Thallium [2, 25, 33–36]

2.2.4 Potentiometric Stripping Voltammetry

In this technique, stirring is crucial in the stripping step to enable the transport of oxidant [30]

$M (Hg) + oxidant \rightarrow Mn^{+}$

As constant anodic current passes through the working electrode to operate, oxidation process. During oxidation, the difference of the working electrode potential is recorded and a stripping peak is achieved. The duration (transition time, t_M) of the oxidation process is quantitative measure of the concentration of the analyte

$t_M \alpha C_{Mn+} td / C_{ox}$

Thus, as the oxidant concentration decreases (C_{ox}), the obtained signal will increase [30].

2.3 Common voltammetric techniques

2.3.1 Cyclic voltammetry (CV)

Cyclic voltammetry is an electrochemical technique for studying and understanding the redox reactions, reaction intermediates and obtaining stability of reaction products. It is characterized by the location of the forward and reverse peaks on the potential axis, the ratio of currents noted on the reverse and forward scans, also, the dependence of peak currents on the scan rate. Cyclic voltammetry can be used in single cycle and multicycle modes [30, 37, 38].

2.3.2 Square Wave Voltammetry (SWV)

The waveform of a square-wave consists of a symmetrical square wave superimposed on a staircase waveform where the forward pulse of the square wave coincides with the staircase

step. The difference between the forward and reverse currents obtained is the net current. The advantages of square wave are speed and high sensitivity. Square wave voltammetry is used for many applications which include the study of electrode kinetics, determination of species at trace levels and electrochemical detection in High Pressure Liquid Chromatography (HPLC) [39].

2.3.3 Differential Pulse Voltammetry (DPV)

Differential Pulse Voltammetry is similar to Normal Pulse Voltammetry, however the only difference is that each potential pulse is fixed of small amplitude from 10-100 mV and is overlayed on a slowly changing base potential. The first current measured is before the pulse and the second is at the end of the pulse. These sampling points are selected to allow for the decay of the charging current. The difference between current measurements at these points for each pulse is determined and plotted against the base potential [40].

2.3.4 Normal Pulse Voltammetry (NPV)

Normal Pulse Voltammetry uses a series of potential pulses of increasing amplitude. The current measurement is made near the end of each pulse. The resulting current equals zero at a certain period. From an initial potential, E_i, the potential is pulsed. The time taken of the pulse, τ, are from 1-100 milliseconds and the interval between pulses are from 0.1-5 seconds. The obtained voltammogram displays the current on the y-axis and the potential to which the pulse is stepped on the x-axis [40].

2.4 Types of electrodes

2.4.1 Mercury electrodes

Due to its high reproducibility, high sensitivity and convenience, hanging mercury drop electrodes (HMDE) has been traditionally used for detecting various heavy metals, organic and inorganic species in stripping voltammetry [27, 41].

Batley and Florence highlighted the advantages of HMDE and MTFE [42]. Based on their research the results obtained for HMDE is reproducible at high concentrations (Sb, Sn, TI, In and Zn) whereas the results obtained for MTFE is reproducible at low concentrations [42].

However, mercury electrodes aren't environmentally friendly thus alternative electrodes are being used which are environmentally friendly and executes high sensitivity. Medvecky and Briancin investigated a method of simultaneous detection of Indium and Gallium by Square Wave Anodic Stripping Voltammetry (SWAdSV) in acetate buffer [20]. The most suitable electrode for simultaneous detection of Indium and Gallium was bismuth thin film electrode or mercury-bismuth thin film electrode. Indium had a high peak potential with Bi-TFE while Gallium preferred the Hg-Bi TFE [20].

2.4.2 Glassy Carbon Electrode

Glassy Carbon Electrodes contains no mercury and has high reproducibility however, obtaining trace levels of heavy metals by the plain electrode is a problem, by modifying the surface of the electrode by metals, nanomaterials or polymers have shown improved limit of detection values [25, 28, 43].

Metal films such as mercury [6, 39] bismuth [10] and antimony [21] have been used to modify the surface of the electrode surface. However, bismuth films are preferred to mercury films, due to bismuth being environmentally friendly, less toxic [27] and also offer better separation between intermetallic compounds than mercury films [27]. Antimony, lead and bismuth films have been

used to determine Indium [21] and Thallium [21, 11, 6]. Bismuth films are further used in other electrode research such as carbon paste [44] and screen printed electrodes[13]. All bismuth electrodes provide a wide potential window of -1.2 to -0.2 V vs. SCE [45].

Recently, the use of metal nanoparticles has been considered as the ideal modifier for the electrode surface due to the unique properties such as large surface to volume ratio, increased mass transport, low detection limit and better signal to noise ratio. Gold nanoparticles modified glassy carbon electrode by anodic stripping voltammetry has been used extensively for detection of arsenic and mercury [25, 28, 46]. Synthesized gold nanoparticles in solution are deposited on the electrode surface by cyclic voltammetry [46].

2.4.3 Carbon Paste Electrode

Carbon paste electrodes are easy to fabricate, non-toxic, inexpensive and environmentally friendly. They have been used in a variety of fields such as detection of catechol in tea leaves [47], heavy metals in water, animals and insecticides [43, 44] paracetamol in pharmaceuticals and urine [14] etc.

Modifying carbon paste electrodes with montmorillonite clay [17, 51–53], graphene [14] ,graphene oxide [15] organically modified silica [52], bismuth [44] and anthraquinone [47] have shown increased detection limits in low levels.

Calcium montmorillonite [53] and sodium montmorillonite (SWy-2) [54] research for detection of lead and mercury, respectively have also being explored. The limit of detection was $1x10^{-10}$ and $6.0x10^{-8}$ mol L^{-1}, respectively.

The use of clays in carbon paste electrodes exhibit many advantages due to properties such as high chemical and mechanical stability, strong adsorption, high cationic exchange capacity and layered structure [55, 49].

The simple construction of the carbon paste electrode involves an insulating liquid (paraffin oil, silicon oil, bromonaphthalene, tricresyl phosphate etc.) mixed with graphene. The mixture is placed inside a plastic tube (carbon paste electrode, syringe, micro pipette tip etc.) with a conducting wire (copper) pushed to the back of the mixture [14]. Each new experiment is done by pushing an excess of the paste out of the tube and polished on weighing paper [14]

2.5 Graphene

2.5.1 Introduction

Graphene is a single sheet of sp^2 hybridized carbon atoms arranged in a honeycomb lattice (Figure 2.1). It has a specific surface area of 2620 m^2/g, Young modulus of 1 TPa, intrinsic strength of 130 GPa, high electronic conductivity at room temperature, electron mobility is $2.5x10^5$ cm^2/Vs and thermal conductivity is around 3000 Wm/K [56]. Due to its unique properties, it has been researched based on its thermal [57], electrical [58], optical [56] and mechanical properties [56].

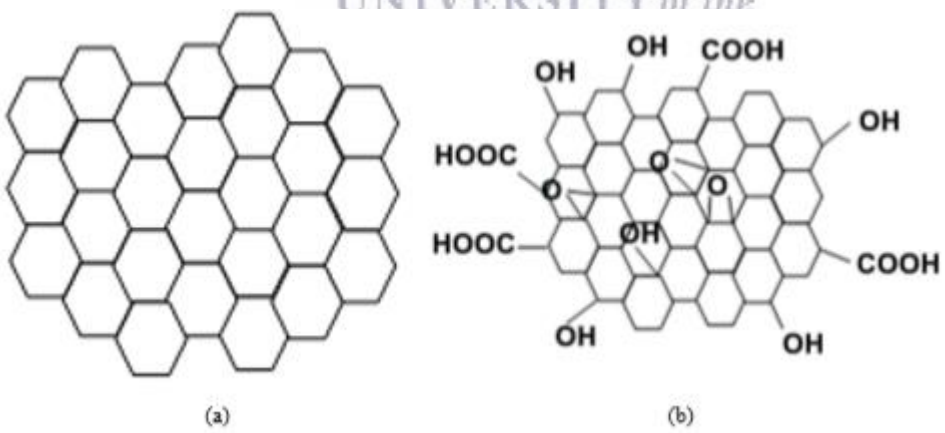

Figure 2. 1: Structure of (a) a single graphene sheet and (b) graphene oxide (GO) [59]

Graphene is used in a variety of applications (Figure 2.2) such as biosensors, polymer composites, transparent electrodes and hydrogen storage [15].

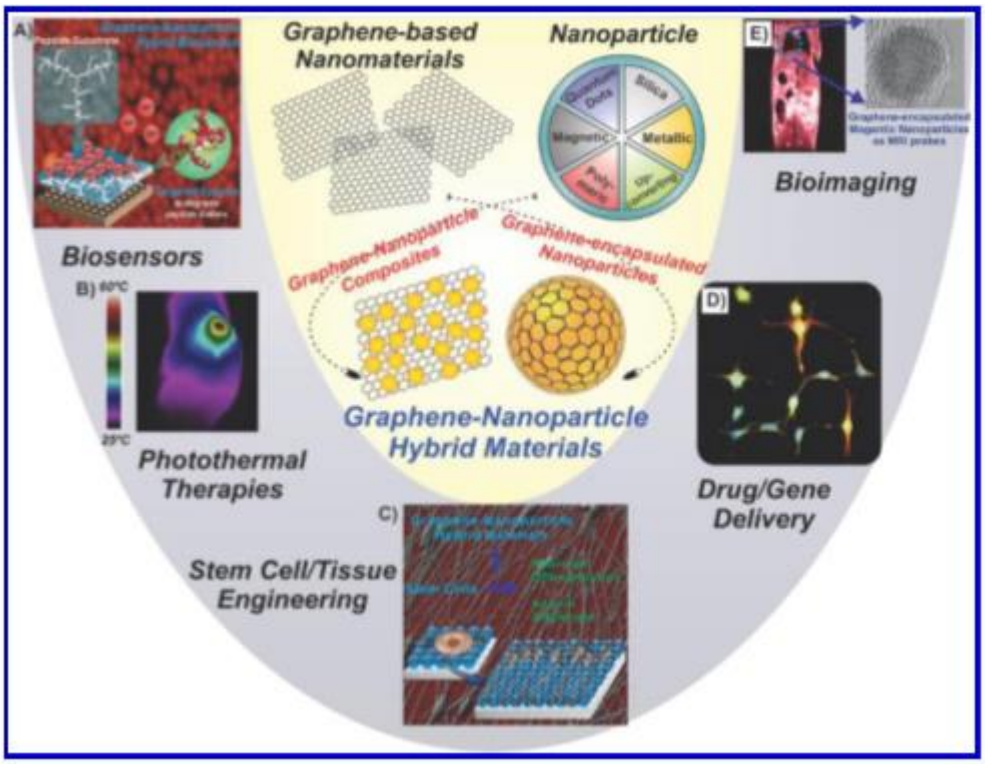

Figure 2. 2: Graphene nanoparticle hybrids exist in two forms, as graphene−nanoparticle composites and graphene-encapsulated nanoparticles, and can be used for various bioapplications including biosensors, photothermal therapies, stem cell/tissue engineering, drug/gene delivery, and bioimaging [60].

Graphite is oxidized to form graphene oxide and then in turn is reduced to produce graphene [11, 61] . The techniques that have been achieved to produce high quality graphene materials include micromechanical cleavage [62], epitaxial growth [62], chemical synthesis through oxidation of graphite, chemical vapour deposition and solvothermal synthesis combined with pyrolysis [63].

These methods were to create single layer of graphene and can be classified into three different routes; mechanical peeling, epitaxial graphene growth and solution based reduction of graphene oxide [63].

2.5.1 Graphene preparation techniques

a) Micromechanical cleavage

Multi-layer graphene is detached from a graphite crystal via scotch tape. Repeated peeling cleaves the multi-layer graphene into various few-layer graphene. The tape is attached to a substrate (SiO_2/Si-wafer) and then removed by acetone. The advantage of this method is the obtained high quality graphene [63, 64] however this method can't be used for mass production [62]

b) Epitaxial growth

Few layer graphene is grown epitaxially on silicon carbide (SiC) by thermal decomposition. To detach the Si atoms from the substrate, they are annealed at temperatures above 1100°C, leaving the C atoms behind which then naturally forms few layer graphene [64].

c) Chemical vapour deposition

For the production of high quality graphene at large scale, chemical vapour deposition is used [65, 58]. The process involves introducing gaseous reactants (methane) onto a substrate (Ni or Cu) in a reaction chamber. The reaction chamber is heated and this causes the gaseous reactants to interact with the substrate, which then creates a material film on the surface of the substrate. Even though this technique obtains high quality graphene, there are quite a few problems involved namely; the temperature must be correct and kept constant at all times, the separation of graphene from the substrate without any damage to it, production of toxic by-products and unsuccessful uniform layers of graphene [58, 65].

d) Chemical synthesis

Graphene oxide is produced by the oxidation of graphite. The principle methods of synthesizing graphene oxide include the Brodie method, Staudenmaier method and the Hummers method [66, 67]. The Hummers method is used commonly for production of graphene oxide compared to the other two. The Hummers method is more simplified due to replacing potassium chlorate ($KClO_3$) and fuming nitric acid (HNO_3) which was used by Brodie [66] to potassium permanganate ($KMnO_4$) and sodium nitrite ($NaNO_3$) in concentrated sulfuric acid (H_2SO_4) to improve the reaction safety and avoiding the evolution of explosive ClO_2.$KClO_3$. Staudenmaier improved the Brodie method by using concentrated sulfuric acid instead of $KClO_3$, however the reaction required the addition of chlorate [66].

2.5.2 Reduction methods

To produce graphene, it is reduced by thermal, chemical or electrochemically reduced graphene oxide methods. The reduction methods facilitate the removal of oxygen from graphene oxide [68].

a) Thermal reduction

The thermal reduction method involves the heating of graphene oxide at a temperature greater than 2000°C to exfoliate the graphite oxide to graphene. The mechanism of the exfoliation involves the expansion of the carbon monoxide (CO) and carbon dioxide (CO_2) between the graphite oxide. The rapid heating causes the oxygen containing functional groups to detach from the carbon plane into gases which creates huge pressure between the stacks [68, 69].

b) Chemical reduction

The chemical reduction method involves the mixing of graphite oxide and sodium borohydride ($NaBH_4$) and the ultra-sonicated for an hour. During the sonication process, the reduction reaction is indicated by a colour change from brown to black. The mixture is washed repeatedly

with deionized water to remove $NaBH_4$ residues and then finally dried in a vacuum oven at 60°C [68], [69].

c) Electrochemical reduction

The electrochemical reduction method requires a glassy carbon electrode in a phosphate buffer by applying a potential of 1.2 V for 900 s. The reduction peaks appear between -0.8 and -1.4 V with a maximum current of -1.2 V [68].

2.6 Nanoscience

The Royal Society and Royal Academy of Engineering define nanoscience and nanotechnology as the study of phenomena and manipulation of materials at atomic, molecular and macromolecular scales, where properties differ significantly from those at a larger scale. Nanotechnologies are the design, characterization, production and application of structures, devices and systems by controlling shape and size at nanometre scale. Nanomaterials are objects that have at least one dimension in the nanometre scale [70].

2.6.1 Types of nanomaterials

a) Zero dimension (0-D)

Zero dimension nanomaterials are materials that are larger than 100 nm and in all dimensions at the nanoscale. A typical example of a zero-dimension nanomaterial is nanoparticles [70].

b) One dimension (1-D)

One dimension nanomaterials are two dimension at the nanoscale and lead to needle-like materials such as nanotubes, nanowires and nanorods [70].

c) Two dimension (2-D)

Two dimensional nanomaterials are one dimension at the nanoscale and usually deposited on a substrate, such as thin films. These materials can be metallic, ceramic or polymeric [70].

d) Three dimension (3-D)

Three dimensional nanomaterials are bulk materials that is not confined to the nanoscale in any dimension. Examples include DNA and zeolites [70].

There are two approaches for synthesizing nanomaterials namely, top-down and bottom up approach. Top down approach involves breaking down of bulk materials into nano-sized materials using mechanical, chemical and other forms of energy. Examples include attrition or

milling. Bottom up approach involves synthesizing the material from atomic or molecular species, via chemical reactions allowing the species to grow in size. Examples of bottom up processors are sol-gel, chemical vapour deposition and aerosol-based processes.

2.6.2 Applications

Due to its unique physical, chemical and mechanical properties, nanomaterials can be used for a wide variety of applications which may include [56];

a) Next-generation computer chips
b) Kinetic energy penetrators with enhanced lethality
c) Phosphors for high definition television
d) Low cost flat panel display
e) High energy density batteries
f) High sensitivity sensors

Chapter Three:

Methodology

3.1 Introduction

This section includes the instrumentation utilized and experimental procedures in obtaining the relevant data used in this study. A step-wise preparation of sample and electrode procedure is provided.

3.2 Reagents

All chemicals used (Table 3.1) were analytical reagent grade and used without purification. Standard stock solutions (1000 mg L^{-1}) were obtained from Sigma Aldrich.

3.3 Standard solutions

Standard solutions were prepared in polyethylene vials in order to limit absorption onto the inner walls of the vial. Atomic absorption stock solutions of TI^{1+} and In^{3+} (1000 ppm) were diluted with 0.01 M HCl.

3.4 Supporting electrolyte

Glacial acetic acid and sodium acetate was diluted in ultra- pure water and mixed to produce 0.1 M acetate buffer (0.1 M, pH 4.6) which was used as a supporting electrolyte. A pH meter (Metrohm 827 pH) was calibrated to confirm the pH of the acetate buffer.

3.5 Square wave analysis

Square wave analysis was performed using a 797 VA COMPUTRACE instrument (Metrohm, Switzerland) controlled by a personal computer. A three electrochemical system consisting of an electrodeposited graphene oxide carbon paste electrode (ERGO-CPE) served as the working electrode. An Ag/AgCl (saturated KCl) and platinum wire served as the reference and counter electrode, respectively. All experiments were performed in a one compartment 20 mL voltametric cell at room temperature.

The cell, Teflon stirrer, counter electrode and reference electrode were cleaned with ethanol and rinsed with distilled water. 0.1 M acetate buffer (20ml) was pipetted into the voltammetric cell. The voltammogram was recorded by applying a potential from -1.5 to 0.3 V using SWASV with rotating speed (1000 rpm), voltage step (0.005 V) and frequency (50 Hz), deposition time (120 s) and amplitude (0.02 V).

The optimum instrumental parameters were determined by changing one and keeping the remaining ones constant. The effect of the peak heights produced by the current were investigated.

A bare carbon paste electrode submerged in only buffer solution was placed in the cell and a baseline was recorded. This was done to determine if the surface of the electrode was clean and if any contamination is present.

Table 3. 1: Chemical reagents used in this work

Chemicals	Source
Graphite powder	Sigma-Aldrich
Mineral oil	Sigma-Aldrich
Potassium permanganate ($KMnO_4$)	PAL Chemicals
98% Sulfuric acid (H_2SO_4)	KIMIX
85% Phosphoric acid	KIMIX
Hydrogen peroxide (H_2O_2)	Sigma-Aldrich
32% Hydrochloric acid (HCl)	KIMIX
99.9% Ethanol (CH_2CH_3OH)	KIMIX
Sodium acetate	Sigma-Aldrich
Acetic acid	Sigma-Aldrich
Thallium	Sigma-Aldrich
Indium	Sigma-Aldrich

3.6 Preparation of Graphene oxide

Preparation of graphene oxide was prepared by the modified Hummer's method. Graphite powder (3 g) was mixed with potassium permanganate (18g). Concentrated sulfuric acid (360 ml) was added to phosphoric acid (40 ml). The concentrated acids were added slowly to the powder mixture. As the mixture was stirred the temperature increased, due to an exothermic reaction. A heater stirrer was used at 50^{o}C with a magnetic stirrer for 12 hours.

After 12 hours, the mixture was cooled down to room temperature. It was poured over deionized ice water (400 ml). An excess of hydrogen peroxide was added with a pipette until a bright yellow colour was obtained. The liquid was poured into measuring tubes and centrifuged for 15 minutes. After centrifuging the liquid was decanted and washed with 10%

HCl and ultra-pure water until the precipitant was basic. It was then dried in a vacuum oven at 70^{o}C for 48 hours. Graphene oxide was grinded into powder using a mortar and pestle.

3.7 Preparation of electrochemical reduced Graphene oxide to form electricochemically-reduced Graphene oxide carbon paste electrodes (ERGO-CPE)

The cyclic voltammetric reduction was performed in 20 ml of GO dispersion (1 mg mL^{-1}) on a 797 VA Computrace instrument in the potential range between -1.4 to +0.3 V for 10 cycles. The instrumental parameters were: deposition time (30 s), deposition potential (-1.4 V), frequency (50 Hz), amplitude (0.02 V) and voltage step (0.005 V).

3.8 Preparation of carbon paste electrodes

Graphite powder (0.5 g) was mixed with mineral oil (182 µL) in a mortar and pestle for 30 minutes until homogenous paste is obtained. The paste was packed in the carbon paste body cavity. The electrode was polished on weighing paper until the excess was removed.

3.9 Characterization techniques

a) Scanning Electron Microscopy

Scanning Electron Microscopy (SEM) measurements were performed using an Auriga SEM 30 kV instrument equipped with Electronic Data System (EDS) and images were taken using the secondary electron detector. The samples were prepared on an aluminium stub which was coated with either Carbon or Iridium.

b) High resolution transmission electron microscopy

High Resolution Transmission Electron Microscopy (HRTEM) measurements were carried out with a Tecnai G2 F20X-Twin MAT Field Emission Transmission Electron Microscope from FEI (Eindhoven, Netherlands) under an acceleration voltage of 200 kV. The samples were prepared by dropping a dilute suspension of graphite or graphene oxide in ethanol onto copper grids followed by air drying at room temperature.

c) Fourier transformed infrared (FT-IR) spectroscopy

A Fourier Transform Infrared (FT-IR) spectrum was recorded using a (Perkin Elmer Spectrum 100) coupled to an Attenuated Total Reflectance (ATR) sample holder. FT-IR was used to obtain information and confirmation on graphite or graphene oxide in the range 4000-1000 cm^{-1}.

d) X-ray diffraction (XRD)

XRD was used to analyse the phase purity and crystalline nature of the graphene oxide [71]. XRD measurements were carried out using a Bruker AXS D8 Advance diffractometer from BRUKER- AXS Germany with Cu-Kα radiation.

e) Raman spectroscopy

Raman and Fourier Transform Infrared Spectroscopy are used to detect vibrations in molecules. They provide information on chemical structures and physical forms to identify substances which is unique to the species being studied [72]. Raman spectroscopy was obtained using a Dilor XY Raman spectrometer with a Coherent Innova 300 Argon laser. Graphite and Graphene oxide was excited with a 514.5 nm laser to enable wavelength absorption. Adhesive glue was used to hold the sample onto the glass slide and then placed onto the stage of the Raman instrument for analysis.

Chapter Four:

Morphology and structural characterization of graphene oxide

4.1 Introduction

This chapter describes and explains the morphological and structural changes of Graphene oxide. HR-SEM, HR-TEM, XRD, FTIR and Raman Spectroscopy were used to confirm the formation of multi-layer graphene oxide sheets to be used as a sensing platform for the detection of Thallium and Indium by Anodic Stripping Voltammetry.

4.2 High-Resolution Scanning electron microscope (HR-SEM)

Scanning electron microscope provides morphology and structure of nanomaterials. The samples prepared for SEM analysis was placed on an aluminium stub and coated with Iridium or Carbon. The HR-SEM images of high grade commercial Graphite and Graphene oxide synthesized by the modified Hummer's method [73] are shown in Figure 4.1 (a and b) and (c and d), respectively. Thin paper-like sheets of Graphite was shown in Figure 4.1 (a and b) at low and high magnification. At higher magnification, the straight, sharp edges of graphite owe to its highly ordered crystalline orientation [13, 73]. From the SEM image in Figure 4.1 (c and d) it's clearly visible that GO has a multiple lamellar layer and the films are stacked one above the other [59]. At a higher magnification in Figure 4.1d , the surface of GO is uneven due to oxidation of sheets [74].

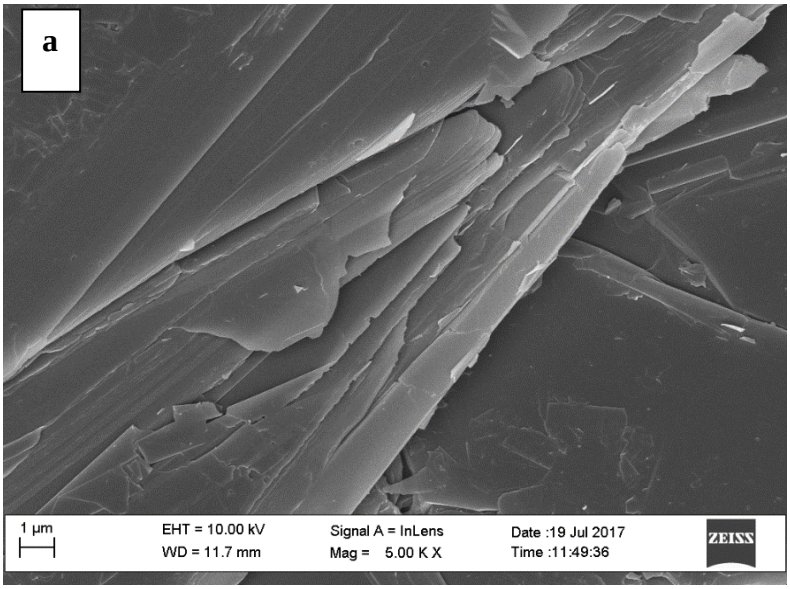

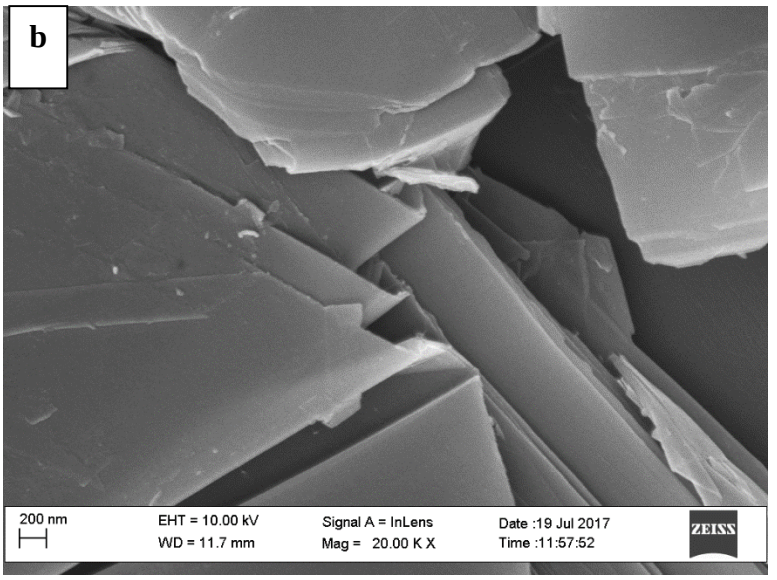

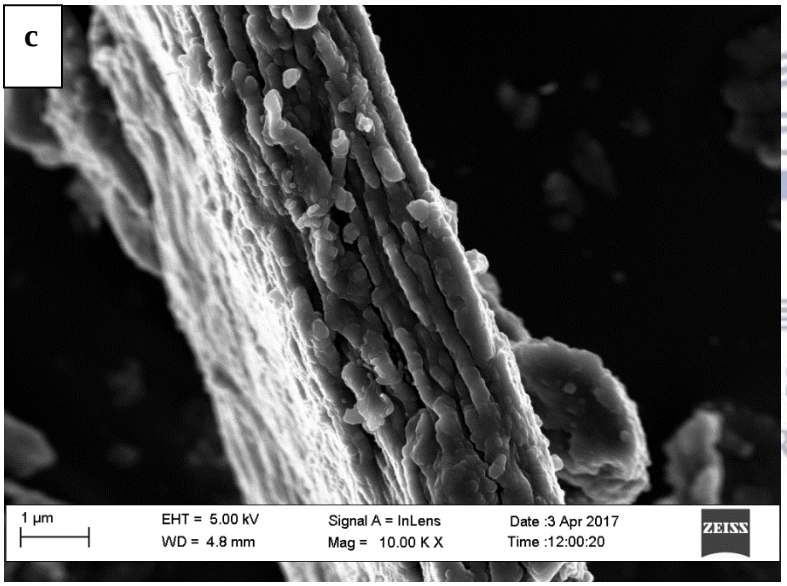

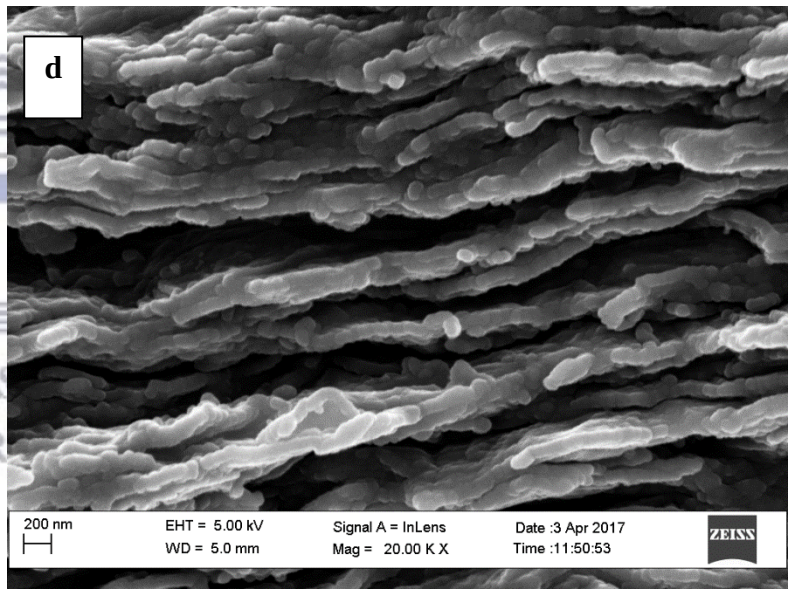

Figure 4. 1: HR-SEM images of (a and b) Graphite and (c and d) Graphene oxide

4.3 High-Resolution Transmission Electron Microscope

Graphite and Graphene oxide samples were prepared by suspension in ethanol, sonicated and then drop casted onto a Cu grid. The surface morphology and crystalline nature of Graphite and Graphene oxide was analysed by HR-TEM in Figure 4.2 (a-d) [71]. In Figure 4.2a straight edges of pure graphite was revealed which suggested a highly ordered crystalline orientation [13]. At higher magnification in Figure 4.2b, the larger and increasingly transparent sheets in graphite resemble wavy silk veils entangled with one another [13]. In Figure 4.2c the edges of GO are thicker due to the oxygen-containing groups [59]. An increase in transparency at higher magnification suggests regions of single layer GO sheets in Figure 4.2d [75].

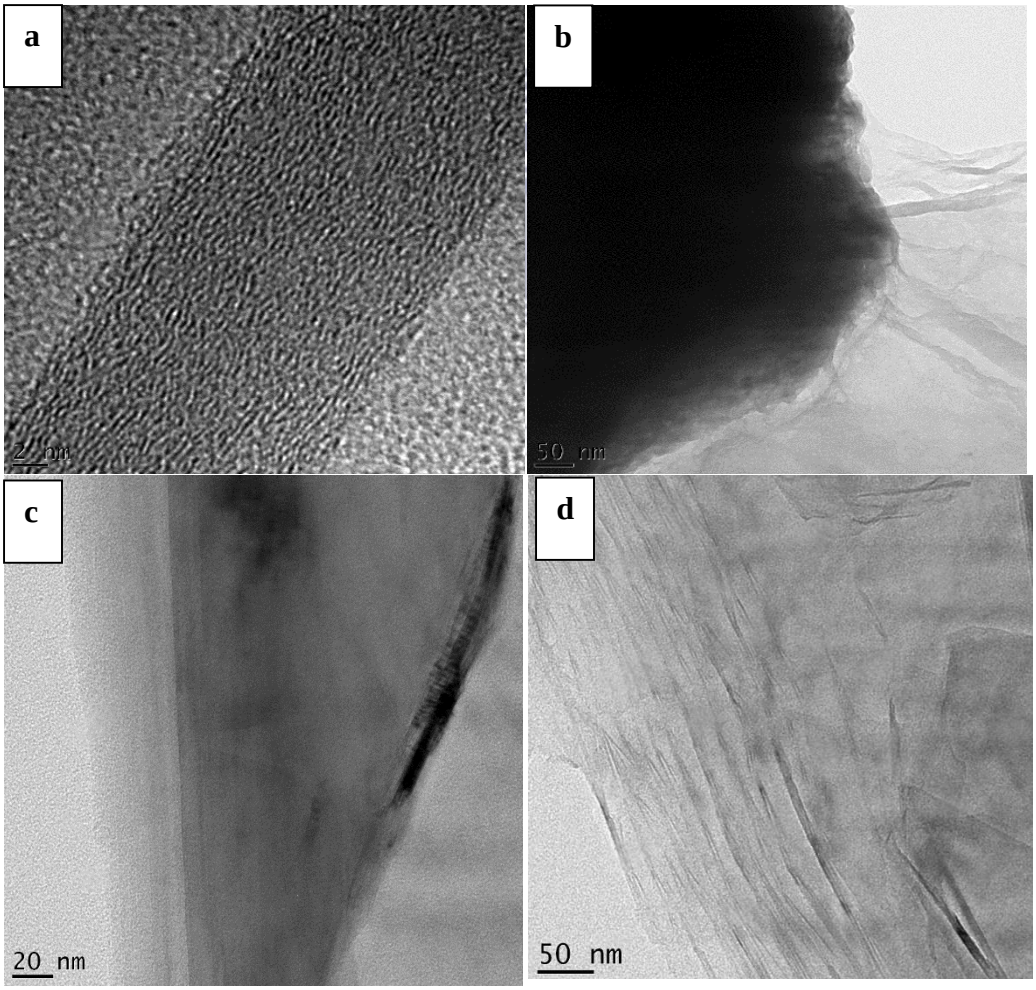

Figure 4. 2: HR-TEM images of (a and b) Graphite and (c and d) Graphene oxide

4.4 X-ray diffraction

X-ray Diffraction (XRD) was used to determine the phase formation and crystallinity [64] of Graphite and Graphene oxide [71]. X-ray diffraction images of Graphite and Graphene oxide are shown in Figure 4.3 (a and b), respectively. The strong, distinct peak at 26.56° as 002 in Figure 4.3a with an inter-planar distance of 0.34 nm using Braggs law indicates a highly ordered carbon structure. The peak indexed as 100 at 43.10° indicates the crystalline structure of graphite [13]. In Figure 4.3b, the appearance of the peak as 001 at 10° results in complete oxidation after chemical oxidation [61] and exfoliation, which indicate an increase in d-spacing from 0.34 nm to 0.82 nm and also [71] due to interlayer spacing which confirms the presence of oxygen functional groups [13, 71]. The broad peak as 002 at 26° indicate an increased disorder, structural defects due to sonication and exfoliated sheets [74, 59]. Similar results are reported in Marcano *et al.* [73].

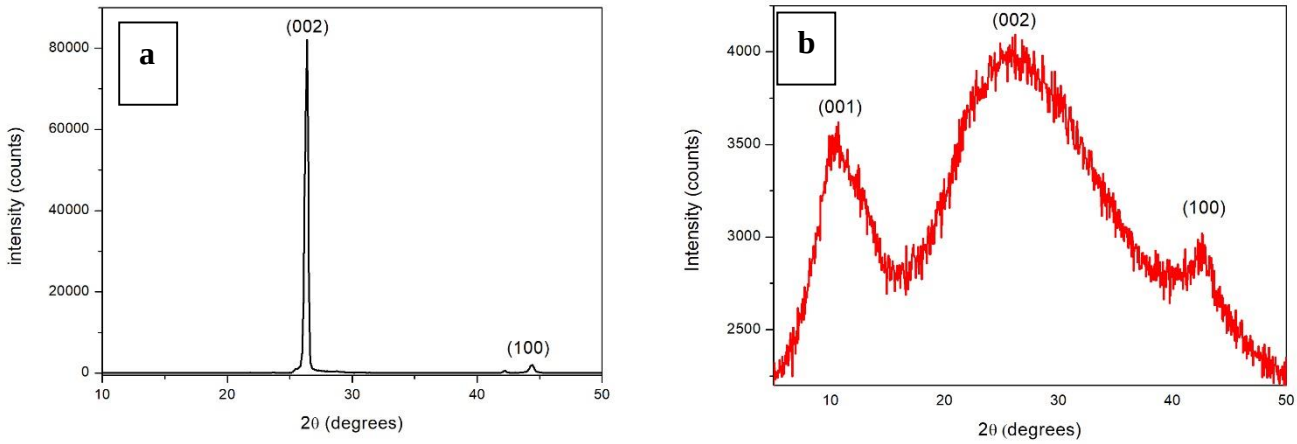

Figure 4. 3: XRD of (a) Graphite and (b) Graphene oxide

4.5 Fourier Transform Infrared Spectroscopy

FTIR analysis was done in order to investigate the structure and functional groups in pure Graphite and Graphene oxide. In Figure 4.4a, pure Graphite revealed no significant functional groups whereas in Figure 4.4b, the broad peak at 3400 cm^{-1} was due to the O-H group present in GO due to the adsorbed water molecules [61] which indicated strong hydrophilicity [73], the carboxyl C=O group appeared at 1720 cm^{-1} due to the edges of GO sheets [71, 76], aromatic C=C groups are present at 1620 cm^{-1} confirms the oxidation of graphite [76]. The stretching vibration of C-O was present at 1050 cm^{-1} which resulted in the oxide functional groups after the oxidation process [61, 69].

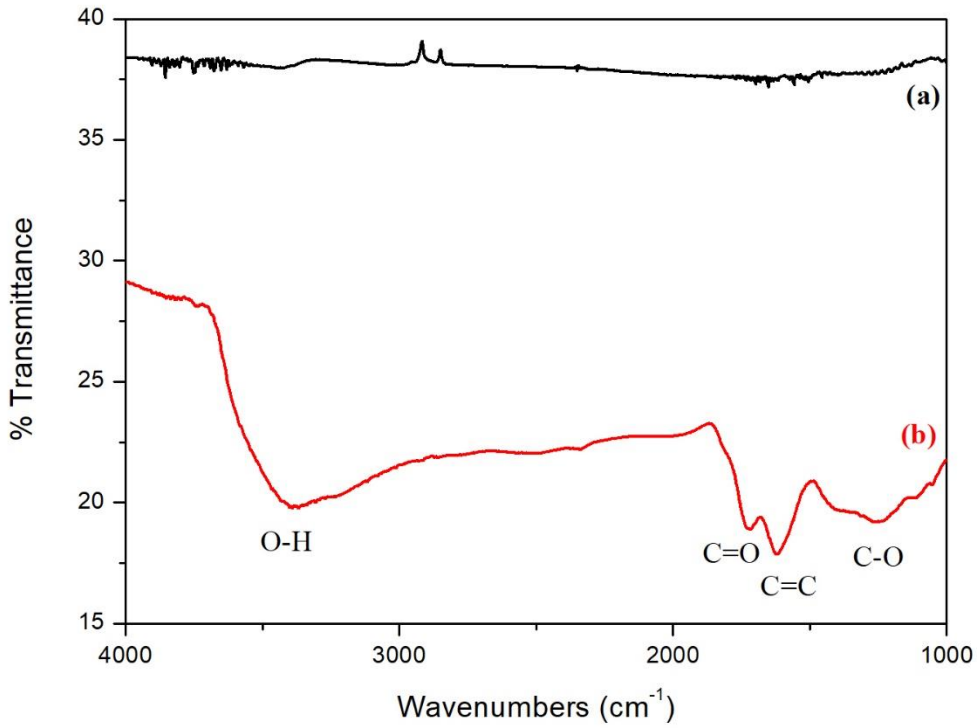

Figure 4. 4: FT-IR spectra of (a) Graphite and (b) Graphene oxide

4.6 Raman Spectroscopy

The change in structure and exfoliation behaviour from graphite to graphene oxide was investigated by Raman spectroscopy and presented by Figure 4.5 (a and b), respectively. The Raman spectra of graphite is shown in Figure 4.5a. The Raman spectra for graphite revealed a sharp G band at 1575 cm^{-1} due to first order scattering of the E_2g mode [56 71] and a significantly weaker D band at 1350 cm^{-1} . The D band is evident for the presence of defects in the graphite material such as bond-angle disorder, bond-length order, vacancies and edge defects [71, 13, 56]. The ratio of the intensities of the D and G bands (I_D/I_G), used as a measure of disorder was calculated as 0.089. The Raman spectra of graphene oxide is shown in Figure 4.5b, showed the D peak located at 1360 cm^{-1} and G peak at 1600 cm^{-1}. The G peak attributes to the in-phase vibration of the sp^2 carbons while the D peak obtained is due to the crystal disorder [56 61, 67]. The calculated I_D/I_G ratio obtained was 0.84, which resulted in an increase in structural disorder [74].

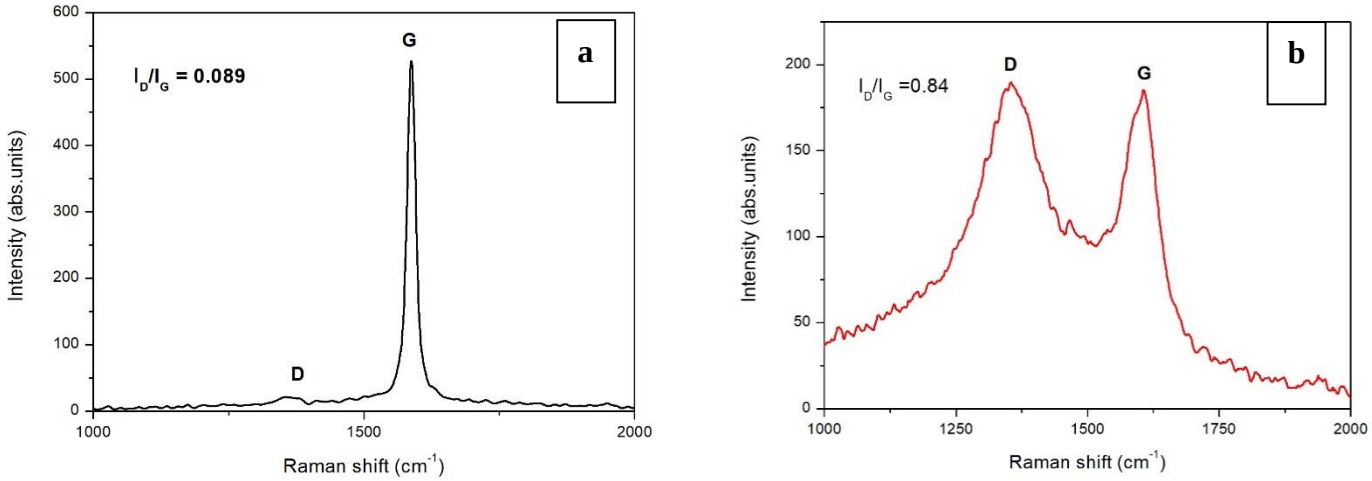

Figure 4. 5: Raman spectrum of (a) Graphite and (b) Graphene oxide

Chapter Five:

Electrochemically-reduced Graphene oxide Carbon Paste Electrodes (ERGO-CPE)

5.1 Introduction

In this chapter an electrochemical reduction technique was used to prepare electrochemically reduced graphene oxide modified carbon paste electrode from graphene oxide solutions. The modified carbon paste electrodes were applied for the determination of TI^{1+} and In^{3+} by Anodic Stripping Voltammetry.

5.2 Electrochemical reduction of graphene oxide

Electrochemically reduced graphene oxide thin films were produced on the carbon paste electrode surface by a direct electrochemical reduction of GO sheets from an aqueous colloidal suspension in acetate buffer solution [13]. Cyclic voltammograms obtained from the electrochemical reduction of a graphene oxide solution (1 mg mL^{-1}) onto CPEs are depicted in Figure 5.1. The cyclic voltammogram show an anodic peak (I) and cathodic peak (II). The redox couple (I and II) confirmed the deposition ERGO on the CPE surface [74]. An increase in anodic peak (I) at 0.2 V with increasing number of scans was observed while the cathodic peak (II) at -0.6 V increases until the fourth cycle then stabilized. The redox behaviour can be appointed to the deposition of ERGO sheets that are formed by the reduction of graphene oxide onto the surface of the electrode [13].

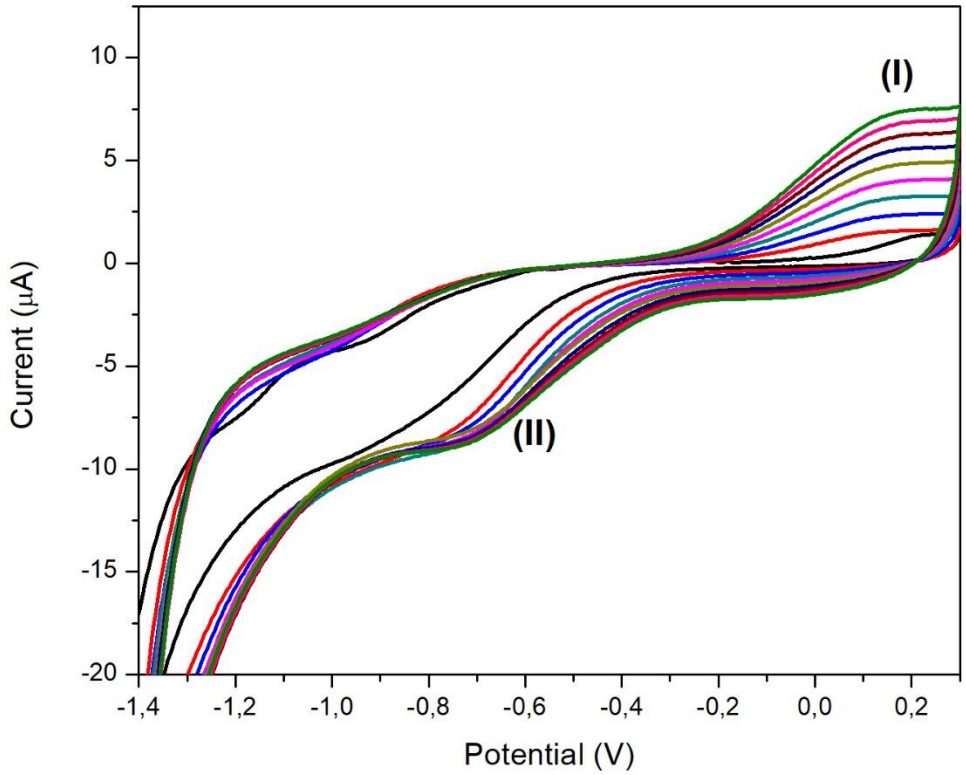

Figure 5. 1: Cyclic voltammograms depicting the electrochemical reduction of 1 mg mL^{-1} GO in acetate buffer solution (0.1 M, pH 4.6) at the CPE at the following instrumental parameters: scan rate (100 mVs^{-1}), deposition time (30 s), frequency (50 Hz), deposition potential (-1.4 V) and voltage step (0.005)

5.3 Electrochemical characterization of the modified carbon paste electrode

Cyclic voltammograms for the unmodified CPE and ERGO-CPE recorded in 0.1 M acetate buffer solution are shown in Figure 5.2. The larger background current of ERGO-CPE compared to the unmodified CPE confirmed the enhanced electronic conductivity and electron transfer of reduced graphene oxide when immobilized at the electrode surface [13].

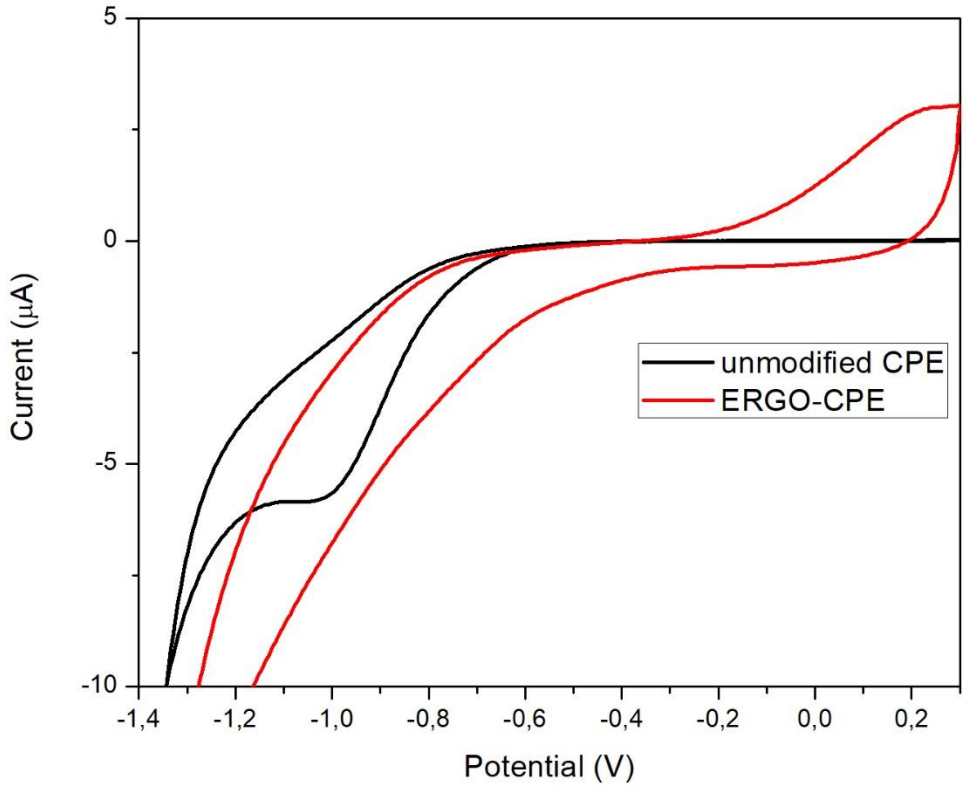

Figure 5. 2: Cyclic voltammograms of unmodified CPE and ERGO-CPE in acetate buffer solution (0.1 M, pH 4.6) at the following instrumental parameters: scan rate (100 mVs^{-1}), deposition time (30 s), frequency (50 Hz), deposition potential (-1.4 V) and voltage step (0.005 V)

5.4 Influence of the number of electrodeposition cycles

The speed and ease of electron transfer through a film is significantly important to the performance and sensitivity of any working electrode [13]. Figure 5.3 showed that the number of electrochemical reduction cycles influenced the stripping peak currents of TI^{1+} and In^{3+}. A general increase in peak currents is observed for TI^{1+} up to 10 cycles, whereas an increase at 15 cycles for In^{3+} was observed. A deposition of ten cycles was selected for TI^{1+} and In^{3+} at ERGO-CPE after which, the thickness of graphene oxide film hinders the flow of electrons to the electrode surface [13].

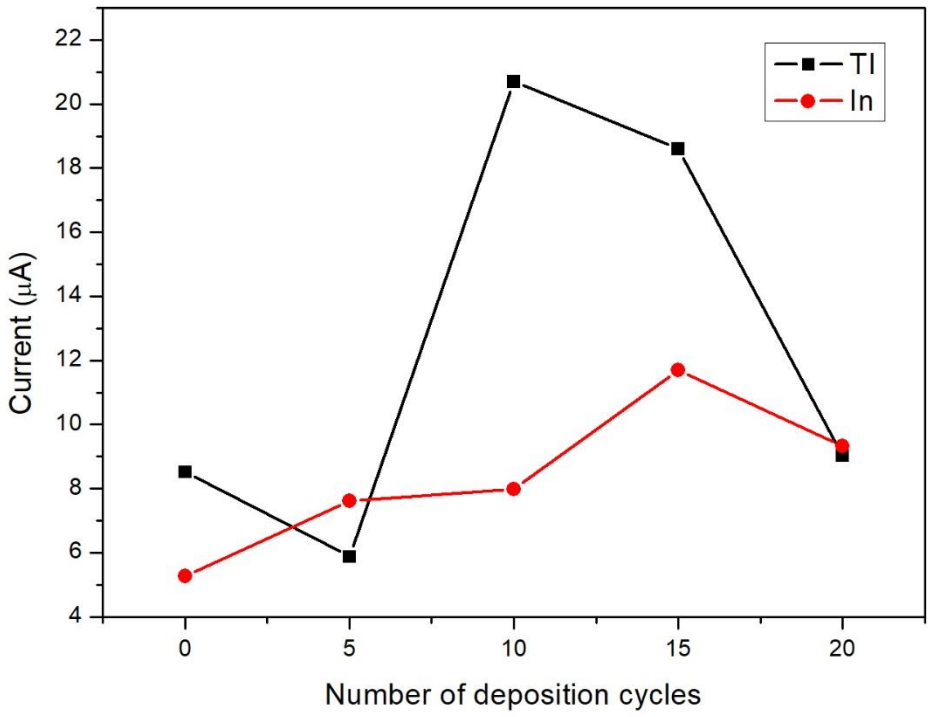

Figure 5. 3: Effect of number of cycles on the stripping peak currents of TI^{1+} and In^{3+} at the ERGO-CPE in 0.1 M acetate buffer (pH 4.6) at 30 s deposition time

5.5 Effect of Electrochemically-reduced Graphene oxide CPEs

The peak current responses of the unmodified CPE and ERGO-CPE towards TI^{1+} and In^{3+} in 0.1 M acetate buffer (pH 4.6) are compared in Figure 5.4. An enhanced peak is observed for TI^{1+} and In^{3+} at the ERGO-CPE in comparison to the unmodified CPE, indicating improved sensitivity towards the heavy metal ions. The higher surface area-to-volume ratio, enhanced electron transfer rates and conductivity owing to quantum confinement of ERGO in the nanometre range (1-100 nm) all contribute towards the improvement in stripping peak current [74]. The oxidation potentials of TI^{1+} and In^{3+} appear at -0.78 and -0.65 V, respectively due to being re-oxidized during the stripping step [74, 13] and result from the redox reactions (Equations 5.1 and 5.2) [13].

Equation 5. 1 $Mn^{n+} + ne^- \rightarrow M$ *(deposition step) (reduction step)*

Equation 5. 2 $M \rightarrow Mn^{n+} + ne^-$ *(stripping step) (oxidation step)*

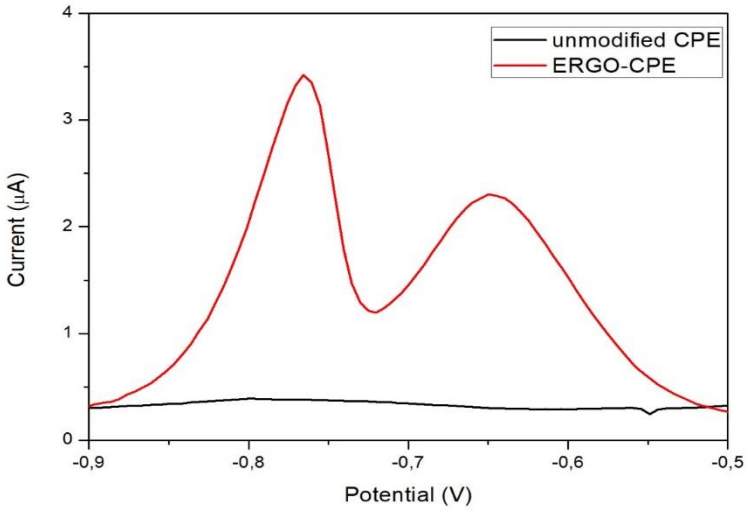

Figure 5. 4: SWASV of 20 μg L^{-1} TI^{1+} and In^{3+} at unmodified CPE and ERGO-CPE. Supporting electrolyte: 0.1 M acetate buffer (pH 4.6), amplitude (0.02 V), frequency (50 Hz), deposition time (120 s), deposition potential (-1.4 V) and rotation speed (1000 rpm).

5.6 Optimization of Instrumental parameters

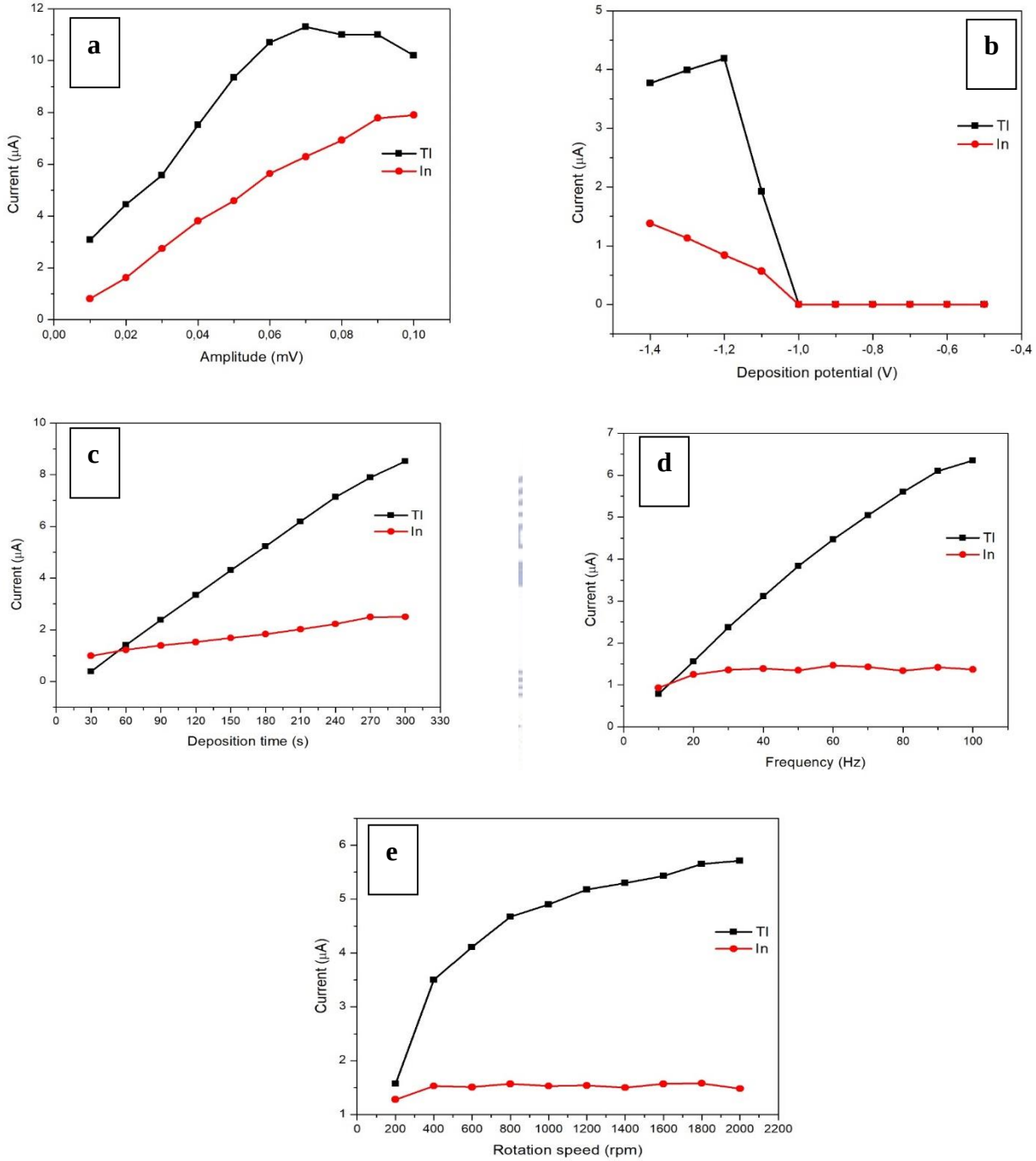

Figure 5. 5: The effect of (a) amplitude, (b) deposition potential, (c) deposition time, (d) frequency and (e) rotation speed on the peak currents of 30 μg L^{-1} of Tl^{1+} and In^{3+} at the ERGO-CPE in supporting electrolyte (0.1 M acetate buffer, pH 4.6).

The square wave parameters affecting the analytical response at the ERGO-CPE are the amplitude, deposition potential, deposition time, frequency and rotation speed and their effect are shown in Figure 5.5.

The influence of amplitude was investigated on the peak currents of TI^{1+} and In^{3+} in the potential range from 0.01 to 0.1 V in Figure 5.5a. The peak currents for TI^{1+} increases as the amplitude increases from 0.01 to 0.07 V, however the peak currents decreased from 0.08 to 0.1 V. The peak currents for In^{3+} increases as the amplitude increases. An optimum of 0.02 V for amplitude was chosen due to no significant increase in peak current with further amplitude increase.

The influence of deposition potential on the peak currents of TI^{1+} and In^{3+} at the ERGO-CPE was studied in the potential range from +0.3 to -1.4 V in Figure 5.5b. At potentials more positive than the oxidation potentials of individual metal ions no stripping peaks were observed at -1.0 V for TI^{1+} and In^{3+} due to the suppression of the reduction reaction responsible for the deposition of metal ions from solution onto the electrode surface. The peak currents for TI^{1+} increases from -1.4 to -1.2 V, due to the preferential reduction and deposition of metal ions at the electrode surface [74, 6], whereas a decrease in peak currents attributes to electrode saturation which is observed for In^{3+} from -1.3 V. A potential of -1.4 V was selected for the optimum.

The deposition time on the peak currents for TI^{1+} and In^{3+} is shown in Figure 5.5c. As the deposition time increased between 30-300 s, the peak currents increased. This is due to more time allowed for the reduction and deposition to occur at the electrode surface [13], [74]. A deposition time of 120 s was chosen for further analysis.

The effect of frequency on the peak currents of TI^{1+} and In^{3+} at the ERGO-CPE was examined in the potential range from 10 to 100 Hz in Figure 5.5d. The peak current for TI^{1+} increased with increasing frequency and is attributed to the increase in scan rate with increasing

frequency, however for In^{3+} it remains more or less constant. A frequency of 50 Hz was chosen as the optimum.

The rotation speed allows for thorough dispersion of the bulk analyte to the electrode surface where reduction occurs. The effect of rotation speed on the peak currents of TI^{1+} and In^{3+} at the ERGO-CPE was studied from 200-2000 rpm in Figure 5.5e. As the square root of the rotation speed increased, the peak currents of TI^{1+} increased. The effect of rotation speed for In^{3+} did not have a significant change in peak currents. A rotation speed of 1000 rpm was selected as the optimum.

5.7 Analytical performance of the electrochemically reduced graphene oxide modified carbon paste electrode (ERGO-CPE)

The analytical performance of ERGO-CPE were investigated by individual and simultaneous analysis of TI^{1+} and In^{3+} over a (5-50 μg L^{-1}) concentration range at Figure 5.6. A slight shift in the peak potentials towards more positive potentials was observed for both metal ions due to the IR-drop effect since the oxidation of the metals became less reversible [13]. Three replicate SWASV measurements were performed for each calibration range. Calibration plots constructed from data obtained from voltammograms were used to calculate the detection limits and are presented in Table 5.1. From the calibration curves in Figure 5.6, the detection limits of the metal ions were determined based on three times the standard deviation of the blank divided by the slope of the calibration curve. The standard deviation of the blank was calculated from ten replications. The detection limits and correlation coefficients for the individual analysis are shown in Table 5.1.

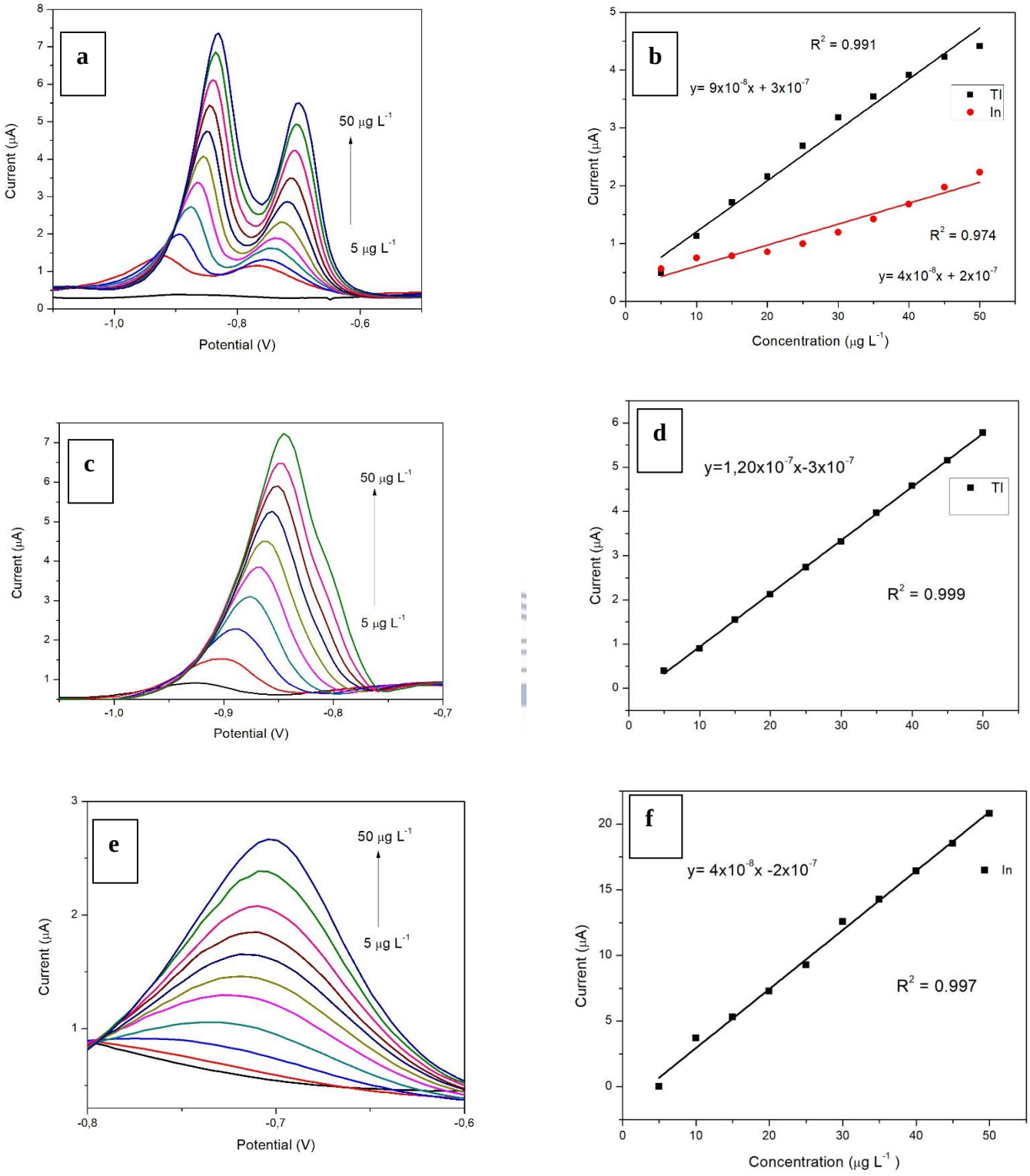

Figure 5. 6: SWASV and calibration plots for simultaneous analysis of TI and In (a and b), TI (c and d) and In (e and f) at ERGO-CPE over 5-50 µg L^{-1} for individual analysis. Supporting electrolyte (0.1 M acetate buffer, pH 4.6), deposition time (120 s), deposition potential (-1.4 V), rotation speed (1000 rpm), frequency (50 Hz), amplitude (0.02 V).

Table 5. 1: Detection limits and correlation coefficients for individual and simultaneous analysis

Individual analysis		
Analytical parameter	TI^{1+}	In^{3+}
Sensitivity (μA L μg $^{-1}$)	$1.2x10^{-7}$	$4x10^{-8}$
Standard deviation of blanks (A)	$3.9x10^{-8}$	$1.57x10^{-7}$
Detection limit (μg L^{-1})	0.975	1.04
Correlation coefficient (R^2)	0.999	0.997
Simultaneous analysis		
Analytical parameter	TI	In
Sensitivity (μA L μg L^{-1})	$9x10^{-8}$	$4x10^{-8}$
Standard deviation of blanks (A)	$3.89x10^{-8}$	$8.9x10^{-8}$
Detection limit (μg L^{-1})	1.32	1.33
Correlation coefficient (R^2)	0.991	0.974

5.8 Recovery studies of ERGO-CPE

Recovery studies on test solutions of TI^{1+} and In^{3+} were investigated at ERGO-CPE by a standard addition method shown in Figure 5.7. 20 mL portions of 0.1 M acetate buffer solution were spiked with known concentrations of target metals. Individual analysis showed improved recoveries compared to the simultaneous analysis, indicating better quantitation for both metals. Recovery percentages of TI^{1+} and In^{3+} ions from test solutions spiked with 10 μg L^{-1} TI^{1+} and In^{3+} for simultaneous analysis yielded a recovery of 90% ± 1.56% and 91% ± 5% , respectively. The recovery percentages for individual analysis of TI^{1+} and In^{3+} spiked with the

same amount as for simultaneous analysis was yielded a recovery of 95% ± 1.3% and 97% ± 6.8%, respectively.

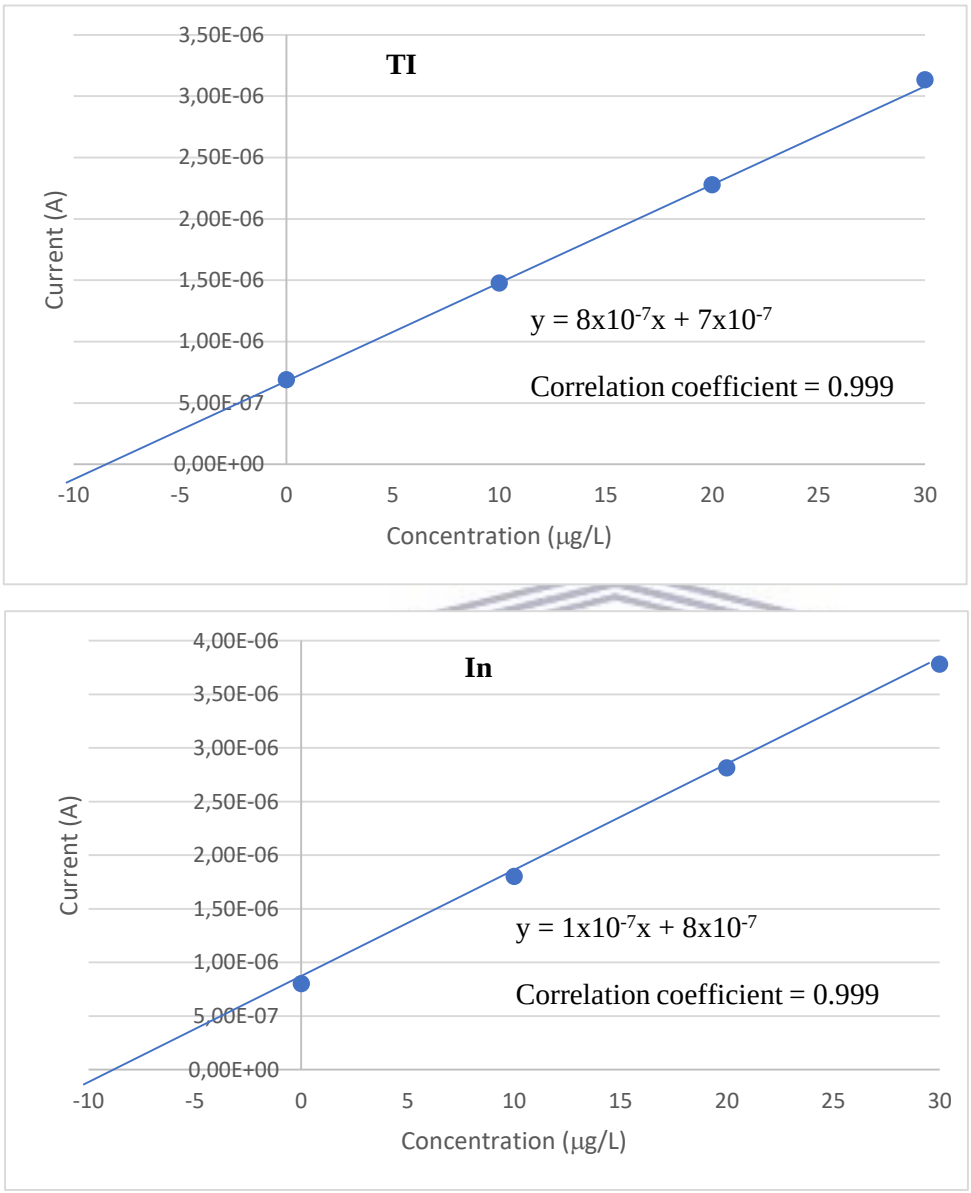

Figure 5. 7: Standard Addition plots for the individual determination (a) TI^{1+} and (b) In^{3+} at ERGO-CPE in test solutions

5.9 Application to real water samples

Tap water samples were collected in the laboratory and analyzed for TI^{1+} and In^{3+} ions using the electrochemically-reduced graphene oxide carbon paste electrode (ERGO-CPE). Individual and simultaneous analysis was performed. The amount of metal ions present in the water samples were quantified by the standard additions method. None of the heavy metal ions were detected in the original tap water samples when using a deposition potential of 120 seconds suggesting that the concentration of the metal ions was below their detection limits. Recovery percentages of TI^{1+} and In^{3+} ions from test solutions spiked with 10 μg L^{-1} TI^{1+} and In^{3+} for simultaneous analysis yielded a recovery of 90% ± 1.6% and 100% ± 8.9% , respectively. The recovery percentages for individual analysis of TI^{1+} and In^{3+} spiked with the same amount as for simultaneous analysis yielded a recovery of 95% ± 2% and 97% ± 7%, respectively. These recoveries show that ERGO-CPE with square wave anodic stripping voltammetry is suitable for monitoring TI^{1+} and In^{3+} in drinking water.

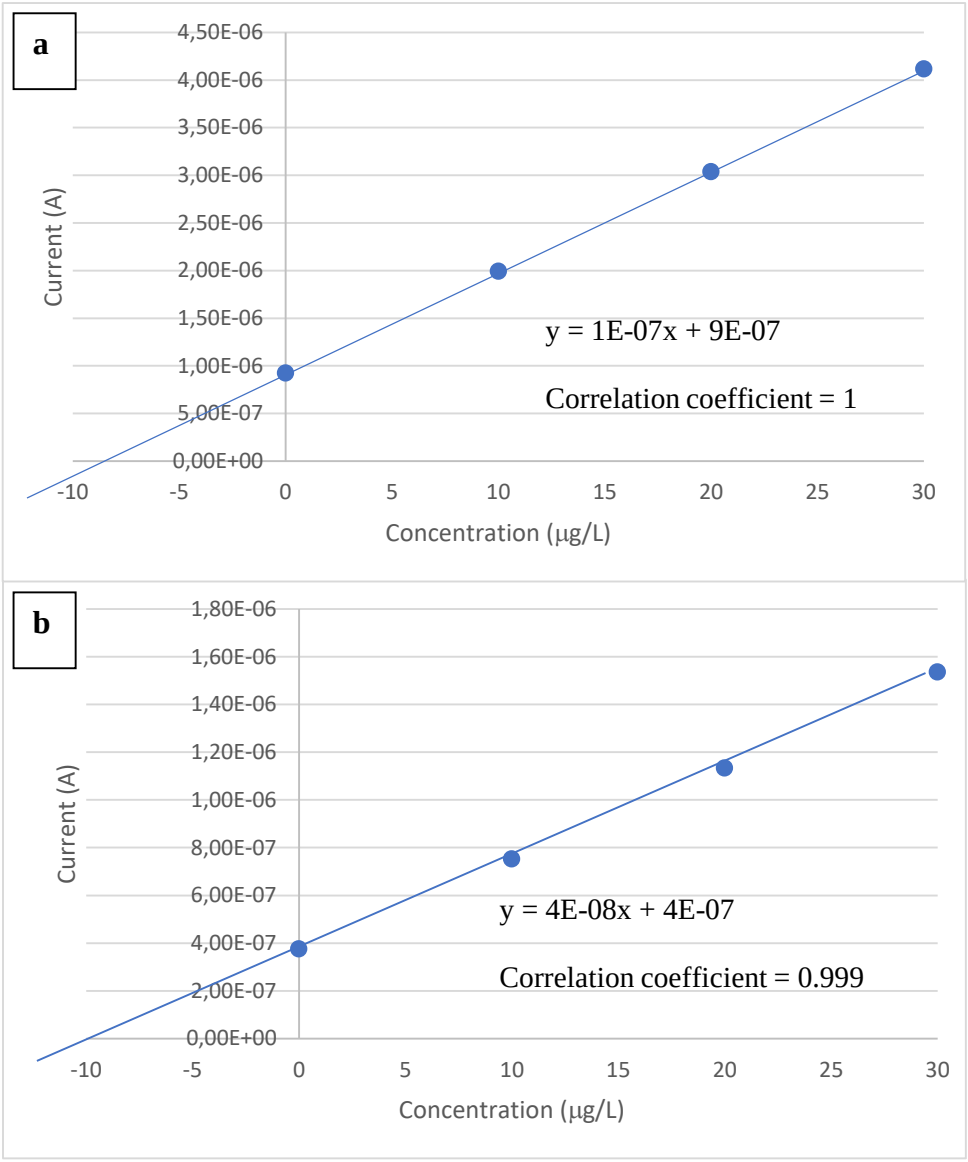

Figure 5. 8: Standard Addition plots for the simultaneous determination (a) TI^{1+} and (b) In^{3+} at ERGO-CPE in real water solutions

5.10 Interference studies

The possible interference of Zn^{2+}, Cd^{2+}, Co^{2+}, Pb^{2+} and Cu^{2+} on the anodic stripping peak of TI^{1+} was investigated individually by the addition of the interfering metal ions between 5-50 μg L^{-1} to a solution containing 5 μg L^{-1} of TI^{1+} under optimized conditions shown in Figure 5.9. Metal ions interfere with the stripping peak by producing reduction peaks that overlap with or even completely suppress the TI^{1+} peak altogether. Zn^{2+}, Co^{2+}, Pb^{2+} and Cu^{2+} did not affect the stripping peaks of TI^{1+}. However, upon the addition of Cd^{2+} caused the stripping peak of TI^{1+} to split due to the oxidation peak potential of Cd at -0.65 V, also the appearance of Zn^{2+} at -1.1 V was present. Possible explanation was due to contamination.

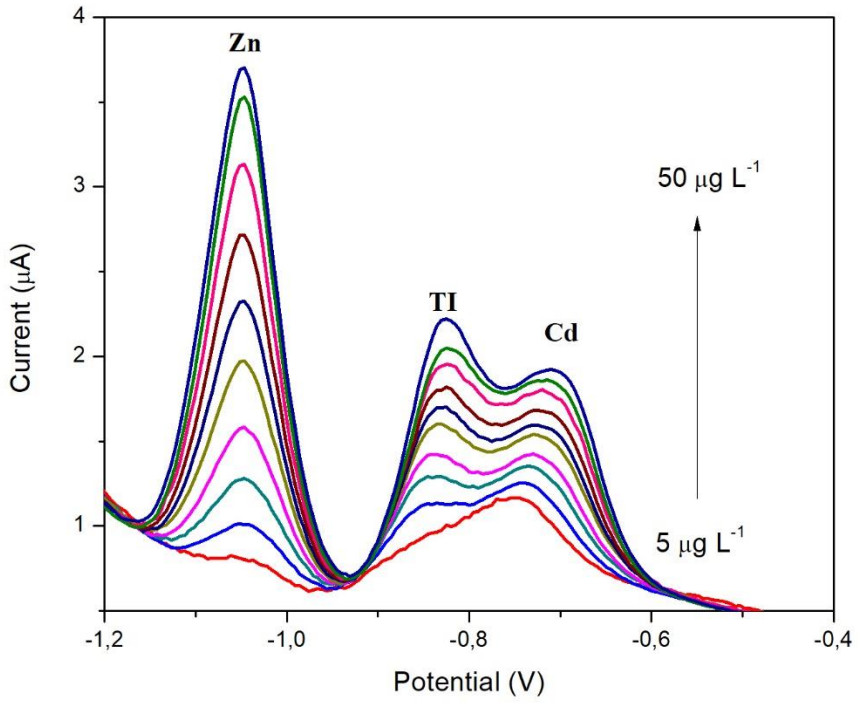

Figure 5. 9: Interference plot for TI^{1+} in the presence of Cd^{2+} in the range (5-50 μg L^{-1}) at ERGO-CPE. Supporting electrolyte (0.1 M acetate buffer, pH 4.6), deposition time (120 s), deposition potential (-1.4 V), rotation speed (1000 rpm), frequency (50 Hz), amplitude (0.02 V)

5.11 Conclusions

The electrochemically-reduced graphene oxide modified carbon paste electrode (ERGO-CPE) resulted in a sensitive sensing platform for the detection of TI^{1+} and In^{3+} by square wave anodic stripping voltammetry. Improved detection limits were achieved compared to previous reported literature in drinking water due to electron transfer rate and surface area to volume ratio due to the graphene oxide. The analytical application of the ERGO-CPE was assessed by recovery studies and real sample analysis within a 10% error.

Chapter Six:

Electrochemically-reduced Graphene Oxide Carbon Paste Mercury film electrodes (ERGO-CP-HgE)

6.1 Introduction

In this chapter the use of SWASV together with an *in situ* mercury film at an electrochemically-reduced carbon paste electrode was investigated for the detection of TI^{1+} and In^{3+} in water samples.

6.2 Influence of the number of electrodeposition cycles

Figure 6.1 shows that the amount of electrochemical reduction cycles have an effect on the stripping peak currents of TI^{1+} and In^{3+}. An increase is observed for TI^{1+} up to 10 cycles and then decreases at 15 and 20 cycles, whereas for In^{3+} it increases at 15 cycles and decreases at 20 cycles. A deposition of 10 cycles was selected for TI^{1+} and 15 cycles was selected for In^{3+} as the optimum number of cycles for the detection of heavy metal ions at the ERGO-CP-HgE.

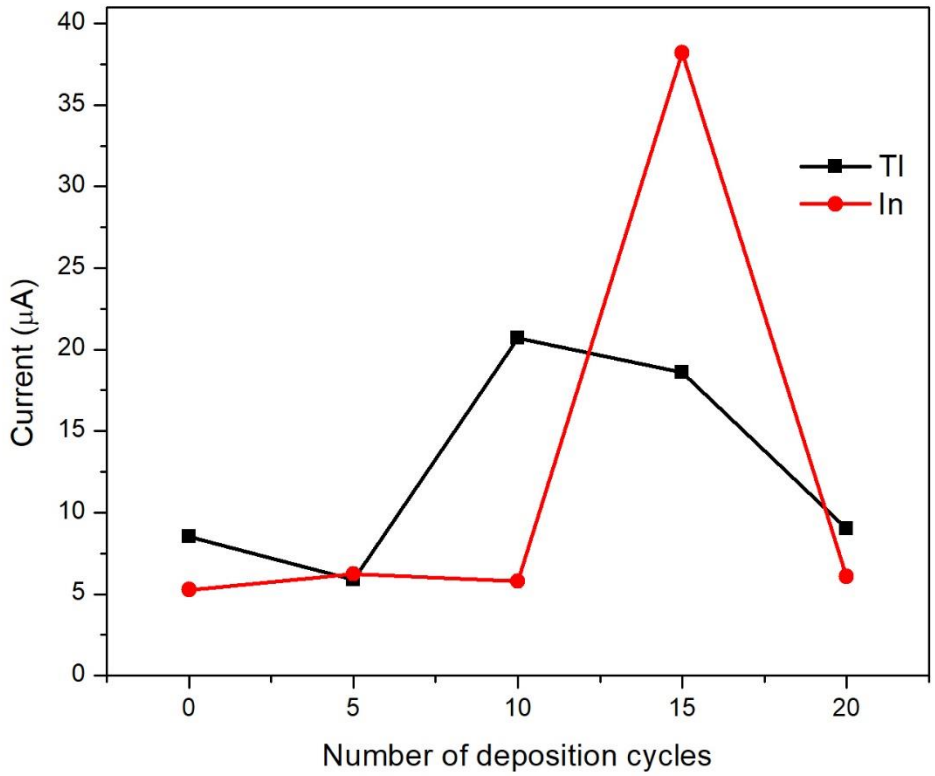

Figure 6. 1: Effect of number of cycles on the stripping peak currents of Tl^{1+} and In^{3+} at the ERGO-CP-HgE in 0.1 M acetate buffer (pH 4.6) at 30 s deposition time

6.3 Effect of Electricochemically-reduced Graphene oxide modified CPEs

The peak current responses of the unmodified CPE and ERGO-CP-HgE towards TI^{1+} and In^{3+} in 0.1 M acetate buffer (pH 4.6) for individual analysis are compared in Figure 6.2 (a and b), respectively An enhanced peak is observed for both TI^{1+} and In^{3+} at the ERGO-CP-HgE in comparison to the unmodified CPE. The oxidation potentials of the metal ions appear at -0.85 V and -0.65 V, respectively for TI^{1+} and In^{3+} and result from the redox reactions (equations 6.1 and 6.2). Simultaneous analysis was not possible due to the positive shift of the peak current of Thallium in the presence of mercury, which resulted in a merged peak rather than two separate peaks which is shown in Figure 6.3. Due to this, no further simultaneous analysis was carried out in this research.

Equation 6. 1 $Mn^{n+} + ne^- + Hg^{2+} \rightarrow M(Hg)$ (deposition step) (reduction reaction)

Equation 6. 2 $M(Hg) \rightarrow Mn^{n+} + ne^- + Hg^{2+}$ (stripping step) (oxidation reaction)

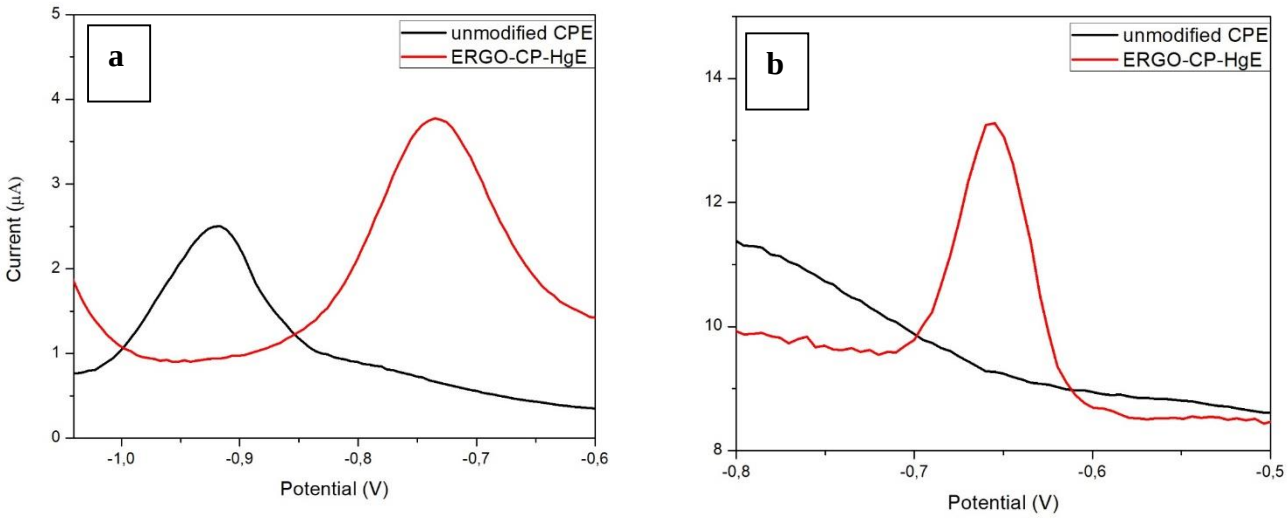

Figure 6. 2: SWASV of 30 μg L^{-1} (a) TI^{1+} and (b) In^{3+} at unmodified CPE and ERGO-CP-HgE .Supporting electrolyte: 0.1 M acetate buffer (pH 4.6), amplitude (0.02 V), frequency (50 Hz), deposition time (120 s), deposition potential (-1.3 V) and rotation speed (1000 rpm).

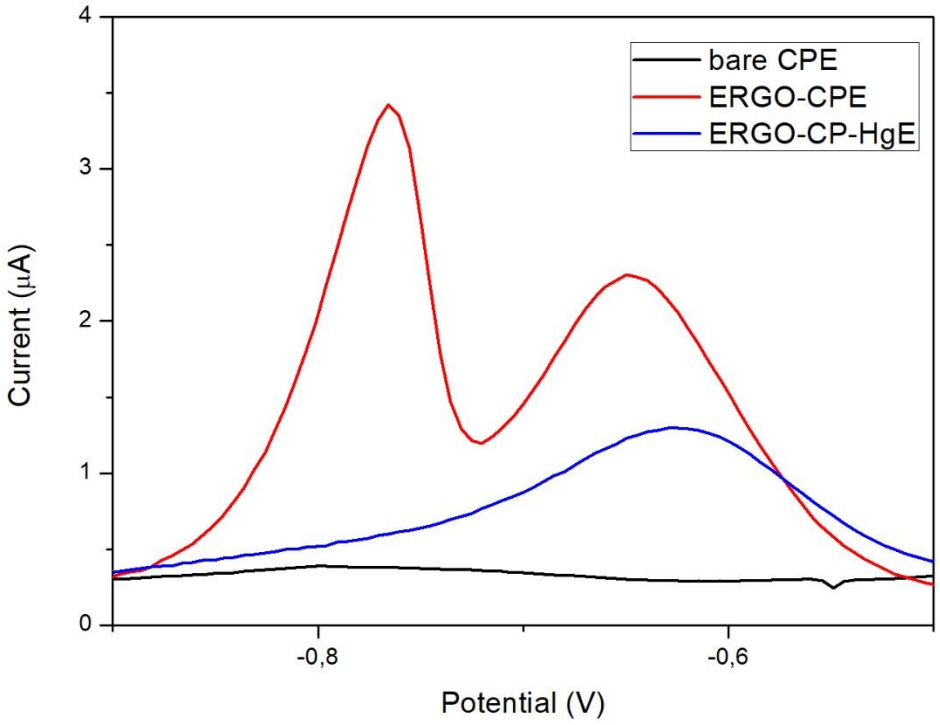

Figure 6. 3: SWASV of 20 μg L^{-1} Tl^{1+} and In^{3+} at bare CPE, ERGO-CPE and ERGO-CP-HgE .Supporting electrolyte: 0.1 M acetate buffer (pH 4.6), amplitude (0.02 V), frequency (50 Hz), deposition time (120 s), deposition potential (-1.3 V) and rotation speed (1000 rpm).

6.4 Effect of the mercury ion (Hg^{2+}) concentration

The influence of the mercury ion concentration leading to mercury film formation at the surface of the unmodified CPE was studied in a 0.1 M acetate buffer solution (pH 4.6) containing 30 µg L^{-1} each of Tl^{1+} and In^{3+}. The stripping peak currents in Figure 6.4 shows an increase for In^{3+} as the Hg^{2+} ion concentration increased from 500 – 5000 µg L^{-1} . For In^{3+} the concentration of Hg film is directly proportional to the thickness of the Hg film [13]. However, for Tl^{1+} the stripping peak currents do not increase but maintain a plateau with increasing Hg^{2+} ion concentration. Due to this behaviour, the mercury concentration of 500 µg L^{-1} for Tl^{1+} and 2000 µg L^{-1} for In^{3+} was chosen.

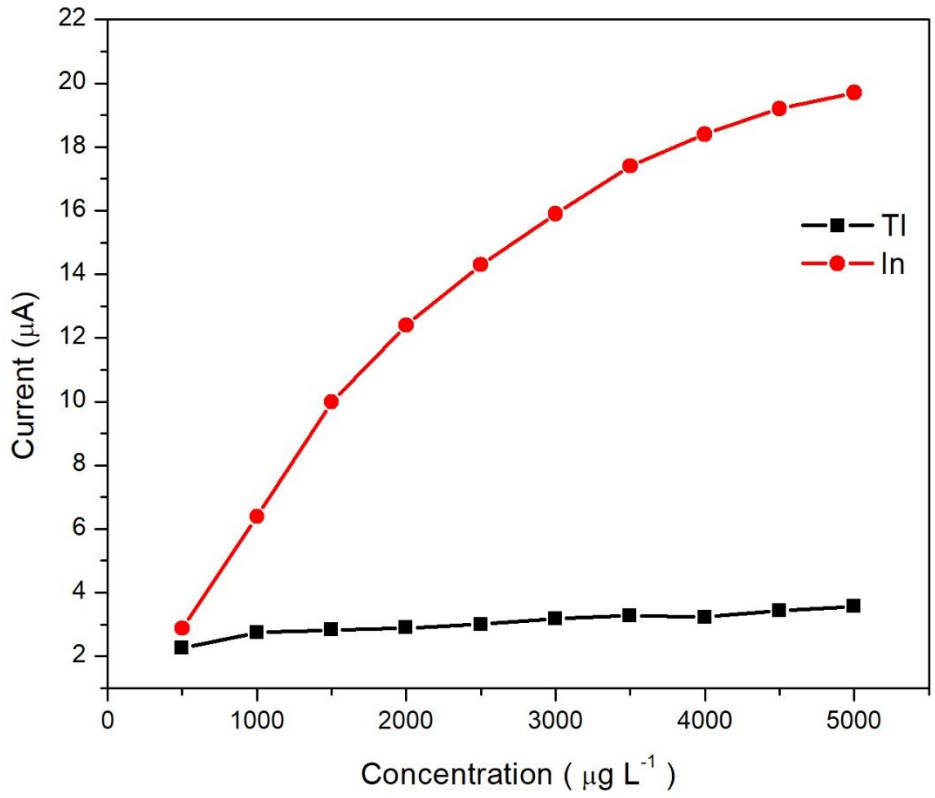

Figure 6. 4: Effect of mercury ion concentration on the stripping peak current of Tl^{1+} and In^{3+} at electrochemically reduced graphene oxide carbon paste mercury film electrode (ERGO-CP-HgE) in a 0.1 M acetate buffer solution (pH 4.6) containing 30 µg L^{-1} of each metal

6.5 Optimisation of Instrumental parameters

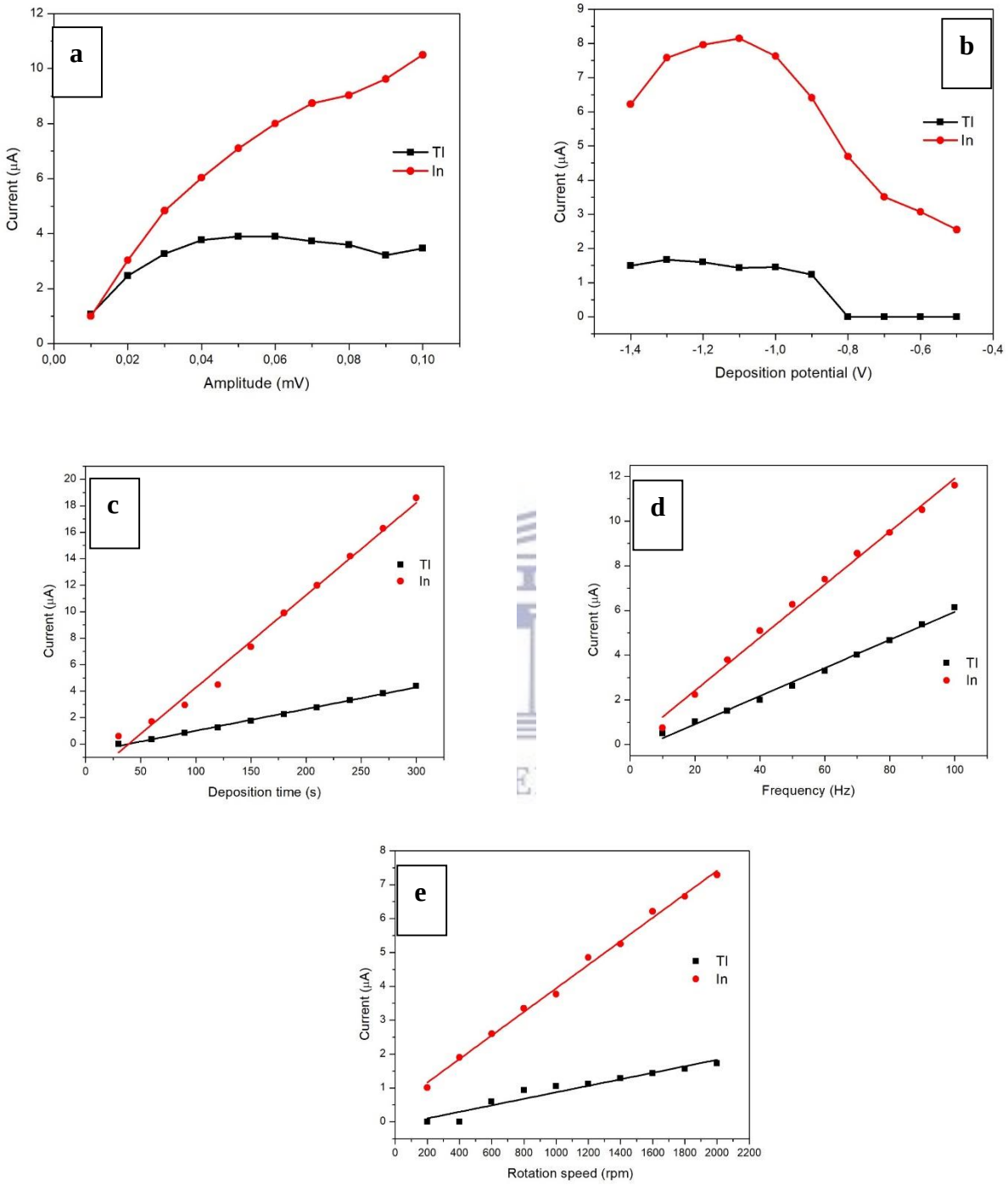

Figure 6. 5: The effect of (a) amplitude, (b) deposition potential, (c) deposition time, (d) frequency and (e) rotation speed on the peak currents of 30 µg L^{-1} of Tl^{1+} and In^{3+} at the ERGO-CP-HgE in supporting electrolyte (0.1 M acetate buffer, pH 4.6)

The influence of amplitude was investigated on the peak currents of TI^{1+} and In^{3+} in the potential range from 0.01 to 0.1 V in Figure 6.5a. As the amplitude increased from 0.01 to 0.05 V, the peak currents for both metals plateaus. An optimum of 0.02 V for amplitude was chosen.

The influence of deposition potential on the peak currents of TI^{1+} and In^{3+} at the ERGO-CP-HgE was studied in the potential range from -0.3 to -1.4 V in Figure 6.5b. The peak current for TI^{1+} gradually plateaus at -1.4 to -0.9 V and decreases from -0.8 to -0.5 V, whereas the peak currents for In^{3+} increases till -1.0 V and gradually decreases from -1.0V onwards. A potential of -1.3V was selected for the optimum for both metals.

The deposition time on the peak currents for TI^{1+} and In^{3+} is shown in Figure 6.5c. As the deposition time increased between 30-300 s, the peak currents increased. This is due to more time allowed for the reduction and deposition to occur at the electrode surface [74]. A deposition time of 120 s was chosen for further analysis for both metals.

The effect of frequency on the peak currents of TI^{1+} and In^{3+} at the ERGO-CP-HgE was examined in the potential range from 10 to 100 Hz in Figure 6.5d. The peak current for TI^{1+} and In^{3+} increased linearly. An increase in the frequency results in an increase of the scan rate. A frequency of 50 Hz was chosen as the optimum.

The effect of rotation speed on the peak currents of TI^{1+} and In^{3+} at the ERGO-CP-HgE was studied from 200-2000 rpm in Figure 6.5e. As the square root of the rotation speed increased, the peak currents of the metals increased. The rotation speed allows for thorough dispersion of the bulk analyte to the electrode surface where reduction occurs [74]. A rotation speed of 1000 rpm was selected as the optimum.

6.6 Analytical performance of the electrochemically reduced graphene oxide modified carbon paste mercury-film electrode (ERGO-CP-HgE)

The analytical performance of ERGO-CP-HgEs were investigated by individual analysis of TI^{1+} and In^{3+} over a concentration range (5-50 μg L^{-1}) . Figures 6.6 show the voltammograms and calibration plots for individual analyses. Calibration plots constructed from data obtained from voltammograms were used to calculate the detection limits and are presented in Table 6.1. From the calibration curves in Figure 6.6, the detection limits of the metal ions were determined based on three times the standard deviation of the blank divided by the slope of the calibration curve. The standard deviation of the blank was calculated from ten replications in the presence of Hg^{2+} ions. A summary of previously reported analyses for TI^{1+} and In^{3+} on various electrodes are shown in Table 6.2.

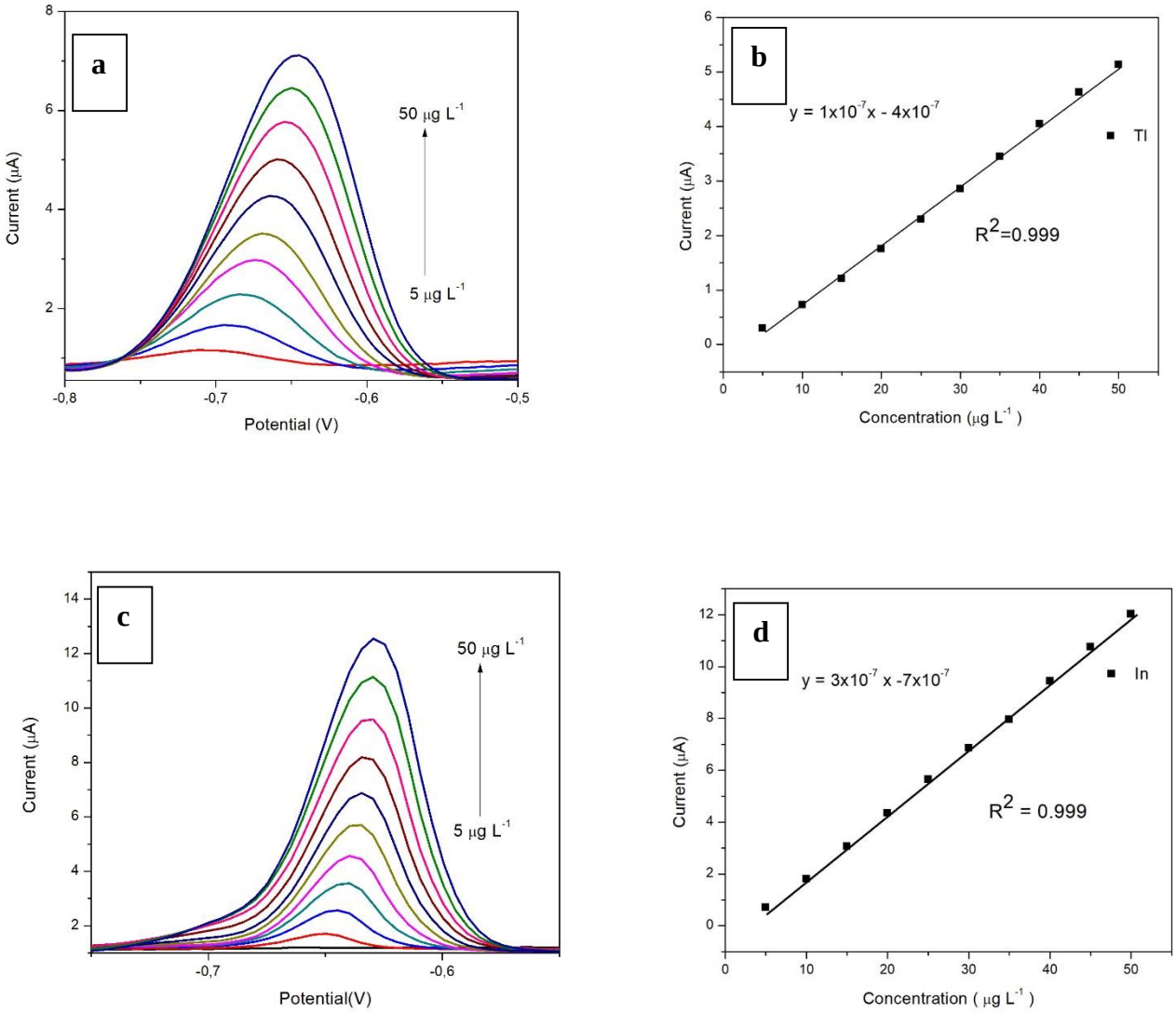

Figure 6. 6: SWASV and calibration plots for individual analysis of (a and b) TI^{1+} and (c and d) In^{3+} at ERGO-CP-HgE over 5-50 µg L^{-1}. Supporting electrolyte (0.1 M acetate buffer, pH 4.6), deposition time (120 s), deposition potential (-1.3 V), rotation speed (1000 rpm), frequency (50 Hz), amplitude (0.02 V)

Table 6. 1: Detection limits and correlation coefficient for individual analysis

Analytical parameter	TI^{1+}	In^{3+}
Sensitivity (μA L μg L^{-1})	$1.10x10^{-7}$	$3x10^{-7}$
Standard deviation of blanks (A)	$8.8x10^{-8}$	$9.76x10^{-8}$
Detection limit (μg L^{-1})	2.4	1.1
Correlation coefficient (R^2)	0.999	0.999

Table 6. 2: Previous reported detection limits for TI^{1+} and In^{3+} at various electrodes

Metals detected	Electrode substrate	Measurement technique	Deposition time (s)	Detection limit ($\mu g\ L^{-1}$)	Reference
Cd, Cu, Pb, Zn, TI, In	Sb-GCE	SWASV	120	Cd = 0.7 Cu = 0.5 Pb = 1.5 Zn = 3.8 TI = 1.0 In = 1.4	[21]
TI and In	Sb-CPE	SWASV	120	TI = 1.4 In = 2.4	[4]
TI and In	Bi-GCE	SWASV	120	TI = 4 In = 2	[12]
TI and In	SbFE	SWASV	120	TI = 2 In = 8	[77]
Thallium	Rotating disc BiFE	SWASV	120	TI = 20	[7]
TI and In	ERGO-CPE (individual analysis)	SWASV	120	TI = 0.975 In = 1.04	[In this work]
TI and In	ERGO-CPE (simultaneous analysis)	SWASV	120	TI = 1.32 In = 1.33	[In this work]
TI and In	ERGO-CP-HgE (individual analysis)	SWASV	120	TI = 2.4 In = 1.1	[In this work]

6.7 Recovery studies of ERGO-CP-HgE

Recovery studies on test solutions of TI^{1+} and In^{3+} were investigated at ERGO-CP-HgE by a standard addition method. 20 mL portions of 0.1 M acetate buffer solution were spiked with known concentrations of target metals. Individual analysis showed improved recoveries, indicating better quantitation for both metals. The recovery percentages for individual analysis of TI^{1+} and In^{3+} spiked with 10 μg L^{-1} yielded a recovery of 80% ± 4.5% and 80% ± 3.9%, respectively. A possible reason for the low recovery percentages achieved is the electrochemical sensor's inability to determine heavy metals simultaneously.

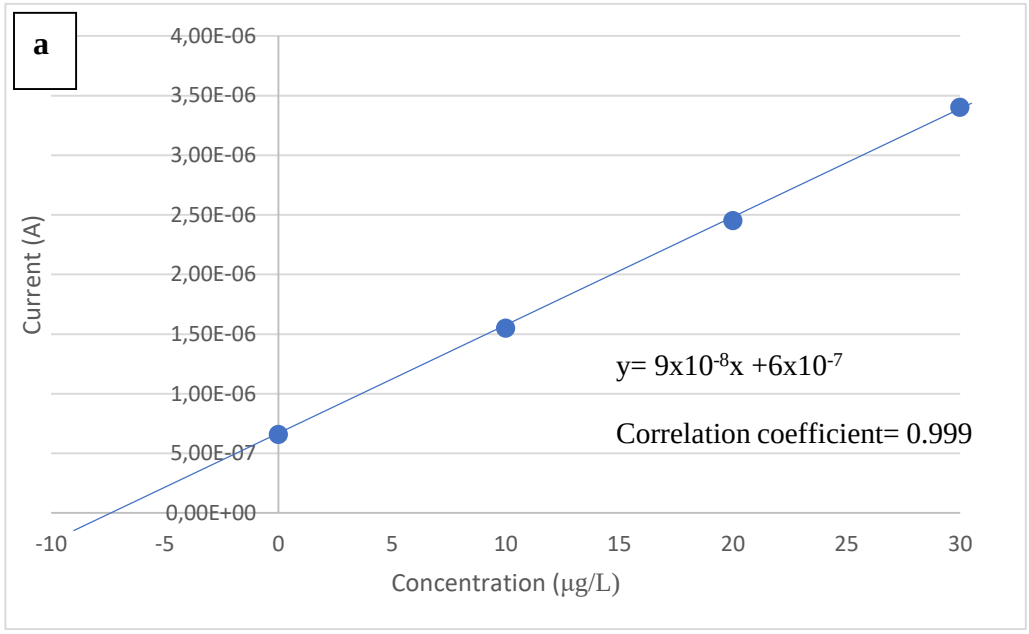

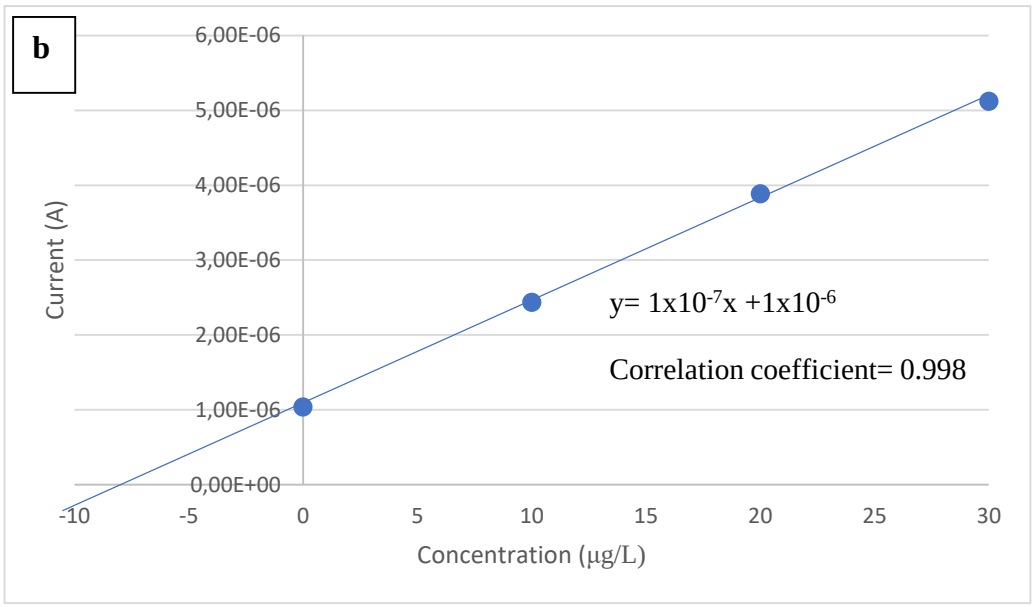

Figure 6. 7: Standard Addition plots for the individual determination (a) TI^{1+} and (b) In^{3+} at ERGO-CP-HgE in test solutions

6.8 Application to tap water samples

Tap water samples were collected in the laboratory and analysed for TI^{1+} and In^{3+} ions using the electrochemically-reduced graphene oxide modified mercury film electrode (ERGO-CP-HgE). Individual analysis was performed and the amount of metal ions present in the water samples were quantified by the standard additions method. None of the heavy metal ions were detected in the original tap water samples when using a deposition potential of 120 seconds suggesting that the concentration of the metal ions was below their detection limits. The recovery percentages for individual analysis of TI^{1+} and In^{3+} spiked with 10 μg L^{-1} yielded a recovery of 80% ± 2.2% and 90% ± 1.95%, respectively. These recoveries show that ERGO-CP-HgE with square wave anodic stripping voltammetry is suitable for monitoring TI^{1+} and In^{3+} in drinking water for individual analysis.

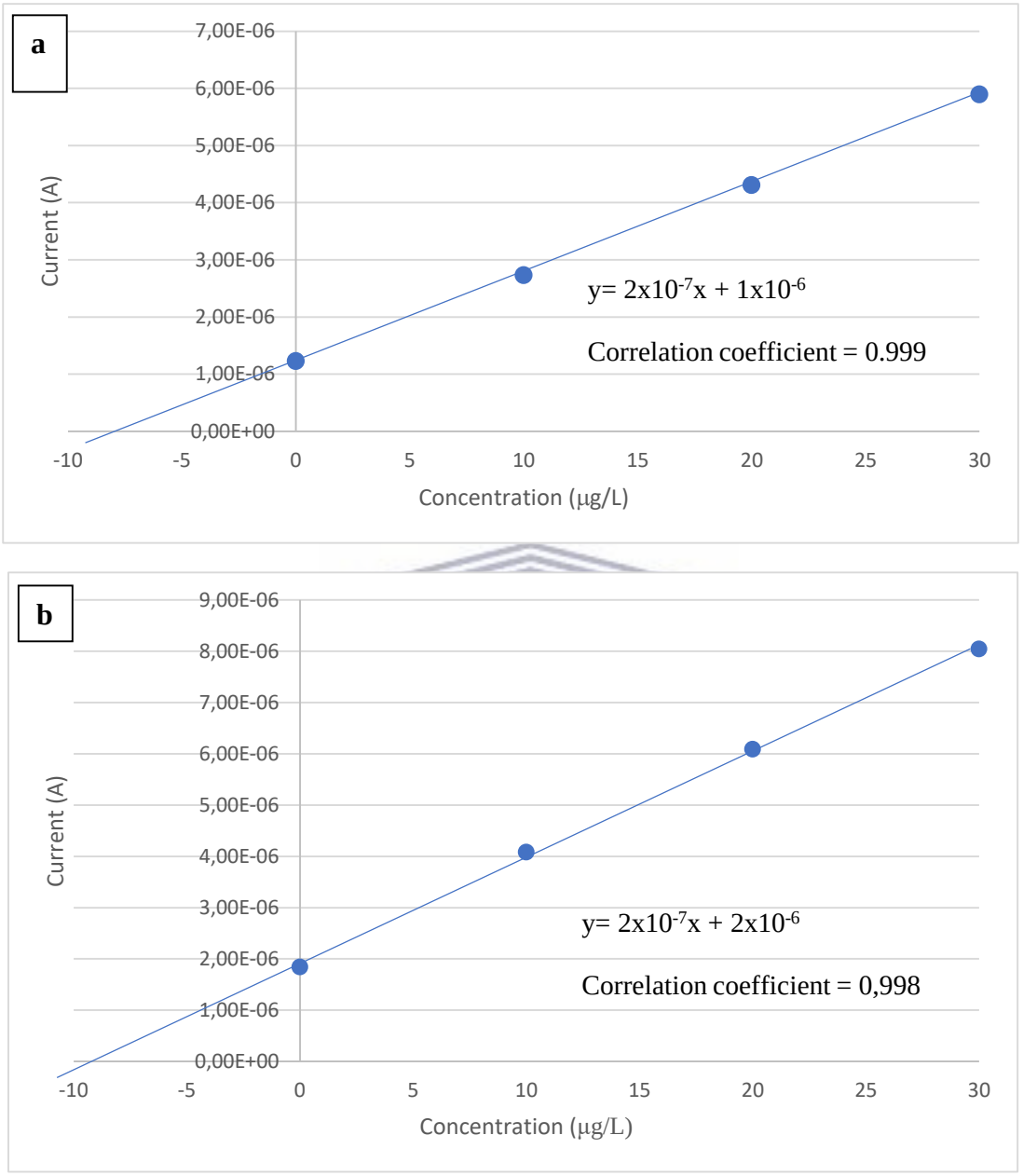

Figure 6. 8: Standard addition plots for the individual analysis of (a) TI^{1+} and (b) In^{3+} at ERGO-CP-HgE in real water samples.

6.9 Interference studies

The possible interference of Zn^{2+}, Cd^{2+}, Co^{2+}, Pb^{2+} and Cu^{2+} on the anodic stripping peak of TI^{1+} was investigated individually by the addition of the interfering metal ions between 5-50 μg L^{-1} to a solution containing 5 μg L^{-1} of TI^{1+} under optimized conditions shown in Figure 6.9. Metal ions interfere with the stripping peak by producing reduction peaks that overlap with or even completely suppress the TI^{1+} peak altogether. Zn^{2+}, Co^{2+}, Pb^{2+} and Cu^{2+} did not affect the stripping peaks of TI^{1+}. However, upon the addition of Cd^{2+} caused the stripping peak of TI^{1+} to split due to the oxidation peak potential of Cd at -0.65 V. This concludes that Cd is an interference towards TI^{1+}.

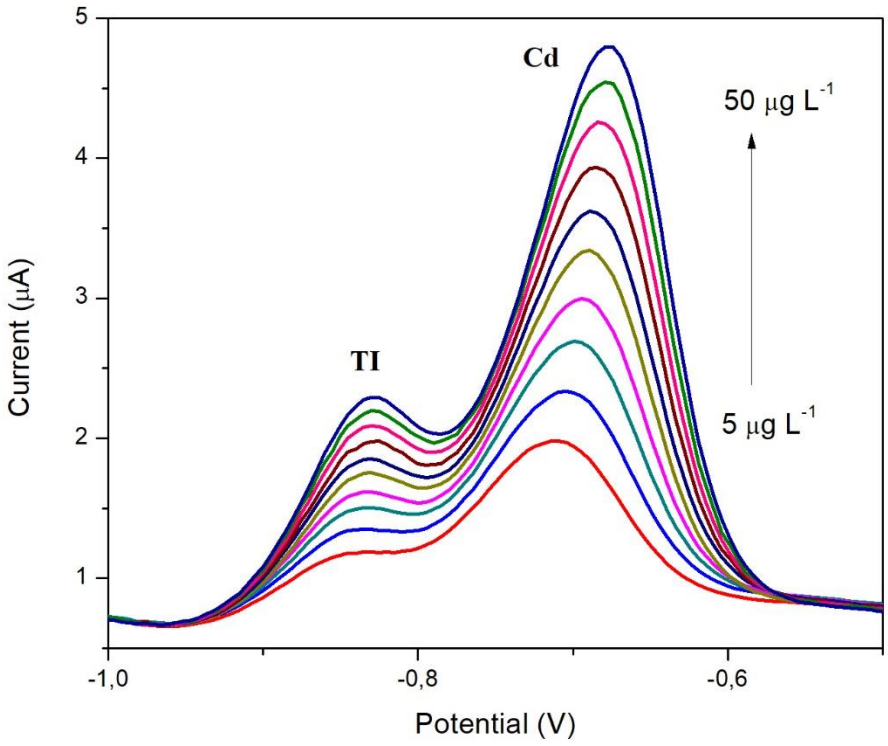

Figure 6. 9: Interference plot of TI^{1+} in the presence of Cd^{2+} in the range (5-50 μg L^{-1}). Supporting electrolyte (0.1 M acetate buffer, pH 4.6), deposition time (120 s), deposition potential (-1.3 V), rotation speed (1000 rpm), frequency (50 Hz), amplitude (0.02 V)

6.10 Conclusions

The electrodeposited graphene oxide carbon paste mercury film electrode (ERGO-CP-HgE) showed good detection limits compared to previous reported literature. The analytical application of the ERGO-CP-HgE was assessed by recovery studies and real sample analysis within a 5% error.

Chapter Seven:

Conclusions and Future Work

7.1 Conclusions

Graphene oxide was synthesized by the modified Hummer's method by oxidizing graphite to graphene oxide by $KMnO_4$ and H_2SO_4. The synthesized nanomaterial was characterized by HR-TEM, HR-SEM, FTIR, Raman and XRD.

The ERGO-CP-HgE was prepared by electro-deposition of graphene oxide onto the surface of the electrode followed by the *in-situ* deposition of mercury thin films. ERGO-CP-HgE was utilized to detect selected heavy metals namely, TI^{1+} and In^{3+}. The instrumental parameters (deposition potential, deposition time, rotation speed, frequency and amplitude) have been optimized. Hence, the deposition potential of -1.3 V, deposition time of 120 s, rotation speed of 1000 rpm, frequency of 50 Hz and amplitude of 0.02 V were identified as the optimum for the determination of the target metal ions. The detection limits using ERGO-CP-HgE for individual analysis were 2.4 and 1.1 μg L^{-1} for TI^{1+} and In^{3+} , respectively. Simultaneous analysis for TI^{1+} and In^{3+} was not obtained, due to the positive shift in the thallium peak in the presence of mercury. Hence, the simultaneous peak merges into one peak and an analysis for separate peak heights are inconclusive.

When using ERGO-CPE, the detection limits for TI^{1+} and In^{3+} were 0.975 and 1.04 μg L^{-1} for individual analysis. The detection limits for simultaneous analysis for TI^{1+} and In^{3+} were 1.32 and 1.33 μg L^{-1}, respectively.

The ERGO-CPE showed improved detection limits for TI^{1+} and In^{3+}, compared to ERGO-CP-HgE.

The application for real water sample at ERGO-CP-HgE and ERGO-CPE for the determination of the metal ions was performed by standard addition method. ERGO-CPE showed better recoveries compared to ERGO-CP-HgE .

7.2 Future work

The future work in this project will deal with:

The application of the ERGO-CPE on other real samples such as waste water or industrial waste water also, determination of other toxic heavy metals such as Pd, As, etc.

Developing a portable device using screen-printed electrodes (SPE) modified with graphene oxide for the on-site detection of heavy metal ions.

References

1. Honeychurch, K. C. Recent Developments in the Stripping Voltammetric Determination of Indium. *World J. Anal. Chem.* **1,** 8–13 (2013).

2. Jan, A. T., Azam, M., Siddiqui, K., Ali, A. & Choi, I. Heavy Metals and Human Health : Mechanistic Insight into Toxicity and Counter Defense System of Antioxidants. *Int. J. Mol. Sci.* **16,** 29592–29630 (2015).

3. Lee, G. J., Lee, H. M., Uhm, Y. R., Lee, M. K. & Rhee, C. K. Square-wave voltammetric determination of thallium using surface modified thick-film graphite electrode with Bi nanopowder. *Electrochem. commun.* **10,** 1920–1923 (2008).

4. Sopha, H. *et al.* Insights into the simultaneous chronopotentiometric stripping measurement of indium(III), thallium(I) and zinc(II) in acidic medium at the in situ prepared antimony film carbon paste electrode. *Electrochim. Acta* **55,** 7929–7933 (2010).

5. Zou, L., Zhang, Y. & Qin, H. Simultaneous Determination of Thallium and Lead on a Chemically Modified Electrode with Langmuir – Blodgett Film of a p -tert-Butylcalix [4] arene Derivative. *Electroanalysis* **21,** 2563–2568 (2009).

6. Kozina, S. A. Stripping Voltammetry of Thallium at a Film Mercury Electrode. *J. Anal. Chem.* **58,** 1067–1071 (2003).

7. Jorge, E. O., Neto, M. M. M. & Rocha, M. M. A mercury-free electrochemical sensor for the determination of thallium(I) based on the rotating-disc bismuth film electrode. *Talanta* **72,** 1392–1399 (2007).

8. Kokkinos, C., Raptis, I., Economou, A. & Speliotis, T. Disposable micro-fabricated

electrochemical bismuth sensors for the determination of Tl(I) by stripping voltammetry. *Procedia Chem.* **1,** 1039–1042 (2009).

9. Aguilar, J. C., Miguel, E. R. D. S. & Gyves, J. De. Adsorptive stripping voltammetry of In (III) in the presence of pyrogallol red in chloride-acetate media. *J. Mex. Chem. Soc.* **45,** 17–20 (2001).

10. Charalambous, A. & Economou, A. A study on the utility of bismuth-film electrodes for the determination of In(III) in the presence of Pb(II) and Cd(II) by square wave anodic stripping voltammetry. *Anal. Chim. Acta* **547,** 53–58 (2005).

11. Franke, J. P. & de Zeeuw, R. A. Differential pulse anodic stripping voltammetry as a rapid screening technique for heavy metal intoxications. *Arch. Toxicol.* **37,** 47–55 (1976).

12. Wang, J., Lu, J., Anik, Ü., Hocevar, S. B. & Ogorevc, B. Insights into the anodic stripping voltammetric behavior of bismuth film electrodes. *Anal. Chim. Acta* **434,** 29–34 (2001).

13. Pokpas, K., Jahed, N., Tovide, O., Baker, P. G. & Iwuoha, E. I. Nafion-graphene nanocomposite in situ plated bismuth-film electrodes on pencil graphite substrates for the determination of trace heavy metals by anodic stripping voltammetry. *Int. J. Electrochem. Sci.* **9,** 5092–5115 (2014).

14. Bahramipur, H. & Jalali, F. Sensitive determination of paracetamol using a graphene-modified carbon- paste electrode. *African J. Pharm. Pharmacol.* **6,** 1298–1305 (2012).

15. Smarzewska, S. & Ciesielski, W. Application of a Graphene Oxide Carbon Paste Electrode for the Determination of Lead in Rainbow Trout from Central Europe. *Food Anal. Methods* **8,** 635–642 (2015).

16. Beltagi, A. M. Utilization of a montmorillonite-Ca-modified carbon paste electrode for the stripping voltammetric determination of diflunisal in its pharmaceutical formulations and human blood. *J. Appl. Electrochem.* **39,** 2375–2384 (2009).

17. Beltagi, A. M., Ismail, I. M. & Ghoneim, M. M. Square-Wave Adsorptive Cathodic Stripping Voltammeteric Determination of Manganese (II) Using a Carbon Paste Electrode Modified with Montmorillonite Clay. *Am. J. Anal. Chem.* **4,** 197–206 (2013).

18. Devnani, H. & Satsangee, S. P. Green gold nanoparticle modified anthocyanin-based carbon paste electrode for voltammetric determination of heavy metals. *Int. J. Environ. Sci. Technol.* **12,** 1269–1282 (2015).

19. Ashrafi, A. M. & Vytřas, K. Determination of Trace Bismuth (III) by Stripping Voltammetry at Antimony-Coated Carbon Paste Electrode. *Int. J. Electrochem. Sci.* **7,** 68–76 (2012).

20. Medvecký, Ľ. & Briančin, J. Possibilities of Simultaneous Determination of Indium and Gallium in Binary InGa Alloys by Anodic Stripping Voltammetry in Acetate Buffer. *Chem. Pap.* **58,** 93–100 (2004).

21. Bobrowski, A., Putek, M. & Zarebski, J. Antimony Film Electrode Prepared In Situ in Hydrogen Potassium Tartrate in Anodic Stripping Voltammetric Trace Detection of Cd(II), Pb(II), Zn(II), Tl(I), In(III) and Cu(II). *Electroanalysis* **24,** 1071–1078 (2012).

22. DeMars, R. D. Simultaneous Determination of Tin and Indium Using Anodic Stripping Voltammetry. *Anal. Chem.* **34,** 259–262 (1962).

23. Liu, T., Lai, D. & Osterioh, J. Indium as internal standard in Square Wave Anodic Stripping Analysis of Lead in blood with microelectrode arrays. *Anal. Chem.* **69,** 3539–3543 (1997).

24. Barón-Jaimez, Jairo Alberto; Marulanda-Arévalo, José Luddey; Barba-Ortega, J. J. Electrodes friendly with the environment for detect heavy metal. *Dyna* **81,** 122–128 (2014).

25. Meepun, N., Siriket, S. & Dejmanee, S. Adsorptive stripping voltammetry for determination of cadmium in the presence of cupferron on a nafion-coated bismuth film electrode. *Int. J. Electrochem. Sci.* **7,** 10582–10591 (2012).

26. Dai, X., Nekrassova, O., Hyde, M. E. & Compton, R. G. Anodic Stripping Voltammetry of Arsenic (III) Using Gold Nanoparticle-Modified Electrodes. *Anal. Chem.* **76,** 5924–5929 (2004).

27. March, G., Nguyen, T. & Piro, B. Modified Electrodes Used for Electrochemical Detection of Metal Ions in Environmental Analysis. *Biosensors* **5,** 241–275 (2015).

28. Bott, A. Stripping Voltammetry. *Current Separations* **12,** 141–147 (1993).

29. Abollino, O., Giacomino, A., Malandrino, M., Piscionieri, G. & Mentasti, E. Determination of mercury by anodic stripping voltammetry with a gold nanoparticle-modified glassy carbon electrode. *Electroanalysis* **20,** 75–83 (2008).

30. Farghaly, O. a, Hameed, R. S. A. & Abu-Nawwas, A.-A. H. Analytical Application Using Modern Electrochemical Techniques. *Int. J. Electrochem. Sci.* **9,** 3287–3318 (2014).

31. Lucia, M., Campos, A. M. & van den Berg, C. M. G. Determination of copper complexation in sea water by cathodic stripping voltammetry and ligand competition with salicylaldoxime. *Anal. Chim. Acta* **284,** 481–496 (1994).

32. Gledhill, M. & Van den Berg, C. M. G. Determination of complexation of iron (III) with natural organic complexing ligands in seawater using cathodic stripping

voltammetry. *Mar. Chem.* **47,** 41–54 (1994).

33. Arancibia, V., Nagles, E., Gómez, M. & Rojas, C. Speciation of Cr(VI) and Cr(III) in water samples by adsorptive stripping voltammetry in the presence of pyrogallol red applying a selective accumulation potential. *Int. J. Electrochem. Sci.* **7,** 11444–11455 (2012).

34. Rojas, C., Arancibia, V., Gómez, M. & Nagles, E. Adsorptive stripping voltammetric determination of cobalt in the presence of nickel and zinc using pyrogallol red as chelating agent. *Int. J. Electrochem. Sci.* **7,** 979–990 (2012).

35. Kefala, G., Economou, A. & Voulgaropoulos, A. Adsorptive Stripping Voltammetric Determination of Trace Uranium with a Bismuth-Film Electrode Based on the U(VI)→U(V) Reduction Step of the Uranium-Cupferron Complex. *Electroanalysis* **18,** 223–230 (2006).

36. Wang, J., Lu, J., Hocevar, S. B. & Farias, P. A. M. Bismuth-Coated Carbon Electrodes for Anodic Stripping Voltammetry. *Anal. Chem.* **72,** 3218–3222 (2000).

37. Abollino, O., Giacomino, A., Ginepro, M., Malandrino, M. & Zelano, I. Analytical applications of silica-modified electrodes - A comprehensive review. *Electroanalysis* **10,** 727–734 (1998).

38. Krishnan, G. Cyclic voltammetry. 1–35 (2011).

39. Lovrić, Š. K. & Lovrić, M. Square-wave Voltammetry of Two-step Electrode Reaction. *Int. J. Electrochem. Sci* **9,** 435–444 (2014).

40. Kounaves, S. P. in *Handbook of Instrumental Techniques for Analytical Chemistry* 709–726 (1997).

41. Ferreira, M. A. & Barros, A. A. Determination of As(III) and arsenic(V) in natural

waters by cathodic stripping voltammetry at a hanging mercury drop electrode. *Anal. Chim. Acta* **459,** 151–159 (2002).

42. Batley, G. & Florence, T. Determination of Thallium in natural waters by Anodic stripping voltammetry. *Electroanal. Chem. Interfacial Electrochem.* **61,** 205–211 (1975).

43. Tang, Y., Sun, C., Yang, X., Yang, X. & Shen, R. F. Graphene Modified Glassy Carbon Electrode for Determination of Trace Aluminium(III) in Biological Samples. *Int. J. Electrochem. Sci* **8,** 4194–4205 (2013).

44. Pauliukaite, R. *et al.* Carbon paste electrodes modified with Bi2O3 as sensors for the determination of Cd and Pb. *Anal. Bioanal. Chem.* **374,** 1155–1158 (2002).

45. Duwensee, H., Adamovski, M. & Flechsig, G. U. Adsorptive stripping voltammetric detection of daunomycin at mercury and bismuth alloy electrodes. *Int. J. Electrochem. Sci.* **2,** 498–507 (2007).

46. Hezard, T. *et al.* Gold nanoparticles electrodeposited on glassy carbon using cyclic voltammetry : Application to Hg (II) trace analysis. *J. Electroanal. Chem.* **664,** 46–52 (2012).

47. Melak, F., Redi, M., Tessema, M. & Alemayehu, E. Electrochemical determination of catechol in tea samples using anthraquinone modified carbon paste electrode. *Nat. Sci.* **5,** 888–894 (2013).

48. Fischer, E. & Van Den Berg, C. M. G. Anodic stripping voltammetry of lead and cadmium using a mercury film electrode and thiocyanate. *Anal. Chim. Acta* **385,** 273–280 (1999).

49. El-Desoky, H. S. & Ghoneim, M. M. Stripping voltammetric determination of silymarin

in formulations and human blood utilizing bare and modified carbon paste electrodes. *Talanta* **84,** 223–234 (2011).

50. Kula, P. & Navra, Z. Voltammetric copper (II) determination with a montmorillonite-modified carbon paste electrode. *Fresenius. J. Anal. Chem.* **354,** 692–695 (1996).

51. Navr, Z. & Kula, P. Determination of gold using clay modified carbon paste electrode. *Fresenius. J. Anal. Chem.* **367,** 369–372 (2000).

52. Etienne, M., Bessiere, J. & Walcarius, A. Voltammetric detection of copper (II) at a carbon paste electrode containing an organically modifed silica. *Sensors Actuators B Chem.* **76,** 531–538 (2001).

53. Sun, D., Wan, C., Li, G. & Wu, K. Electrochemical determination of lead(II) using a montmorillonite calcium-modified carbon paste electrode. *Microchim. Acta* **158,** 255–260 (2007).

54. Huang, W., Yang, C. & Zhang, S. Anodic stripping voltammetric determination of mercury by use of a sodium montmorillonite-modified carbon-paste electrode. *Anal. Bioanal. Chem.* **374,** 998–1001 (2002).

55. Aglan, R. F., Mohamed, G. G. & Mohamed, H. A. Chemically modified carbon paste electrode for determination of cesium ion by potentiometric method. *Am. J. Anal. Chem.* **3,** 576–586 (2012).

56. Zhu, B. Y. *et al.* Graphene and Graphene Oxide : Synthesis , Properties , and Applications. *Adv. Mater.* **22,** 3906–3924 (2010).

57. Pop, E., Varshney, V. & Roy, A. K. Thermal properties of graphene : Fundamentals and applications. *Mater. Res. Soc.* **37,** 1273–1281 (2012).

58. Wei, D. *et al.* Synthesis of N-Doped Graphene by Chemical Vapor Deposition and Its

Electrical Properties. *Nano Lett.* **9,** 1752–1758 (2009).

59. Alam, S. N., Sharma, N. & Kumar, L. Synthesis of Graphene Oxide (GO) by Modified Hummers Method and Its Thermal Reduction to Obtain Reduced Graphene Oxide (rGO) *. *Graphene* **6,** 1–18 (2017).

60. Yin, P. T., Shah, S., Chhowalla, M. & Lee, K. Design , Synthesis , and Characterization of Graphene − Nanoparticle Hybrid Materials for Bioapplications. *Chem. Rev.* **4,** 1–49 (2014).

61. Paulchamy, B., Arthi, G. & Bd, L. A Simple Approach to Stepwise Synthesis of Graphene Oxide. *Nanomedicine Nanotechnol.* **6,** 2–5 (2015).

62. Zheng, Q. & Kim, J. in *Graphene for Transparent Conductors* 29–38 (2015).

63. Oh, W.-C. & Zhang, F.-J. Preparation and Characterization of Graphene Oxide Reduced From a Mild Chemical Method. *Asian J. Chem.* **23,** 875–879 (2011).

64. Shalaby, A. *et al.* Structural analysis of reduced graphene oxide by transmission electron microscopy. *Bulg. Chem. Commun.* **47,** 291–295 (2015).

65. Krane, N. Preparation of Graphene. *Selected Topics in Physics : Physics of Nanoscale Carbon* 1–5 (2010).

66. Dreyer, D. R., Park, S., Bielawski, W. & Ruoff, R. S. The chemistry of graphene oxide. *Chem. Soc. Rev.* **39,** 228–240 (2010).

67. Pavoski, G. *et al.* Few Layer Reduced Graphene Oxide : Evaluation of the Best Experimental Conditions for Easy Production. *Mater. Res.* **20,** 53–61 (2017).

68. Pei, S. & Cheng, H. The reduction of graphene oxide. *Carbon N. Y.* 1–19 (2011).

69. Song, J., Wang, X. & Chang, C. Preparation and Characterization of Graphene Oxide.

J. Nanomater. **2014,** 1–6 (2014).

70. Otto, D. P. & Villiers, M. M. De. Why is the nanoscale special (or not) ? Fundamental properties and how it relates to the design of nano-enabled drug delivery systems. *Nanotechnol. Rev.* **2,** 171–199 (2013).

71. Krishnamoorthy, K., Veerapandian, M., Yun, K. & Kim, S. The chemical and structural analysis of graphene oxide with different degrees of oxidation. *Carbon N. Y.* **53,** 38–49 (2012).

72. Childres, I., Jauregui, L. A., Park, W., Cao, H. & Chen, Y. P. in 1–20 (2013).

73. Marcano, D. C. *et al.* Improved Synthesis of Graphene Oxide. *ACS Nano* **4,** 4806–4814 (2010).

74. Zbeda, S. *et al.* Few-layer Binder Free Graphene Modified Mercury Film Electrode for Trace Metal Analysis by Square Wave Anodic Stripping Voltammetry. *Int. J. Electrochem. Sci* **8,** 11125–11141 (2013).

75. Galpaya, D. Synthesis, Characterization and Applications of Graphene oxide-polymer nanocomposites. (Queensland University of Technology, 2015).

76. Jahanshahi, M., Rashidi, A. M. & Ghoreyshi, A. A. Synthesis and Characterization of Thermally-Reduced Graphene. *Iran. J. Energy Environ.* **4,** 53–59 (2013).

77. Zhang, J., Shan, Y., Ma, J. X. & Li Du, X. Simultaneous determination of Indium and Thallium ions by Anodic Stripping Voltammetry using antimony film electrode. *Sens. Lett.* **7,** 605–608 (2009).